Dynamic and Thermal Analysis of Sandstorm Processes Based on Vertical Observation Data

Yifei Wang[1,2,3,4,5], Wen Huo[1,3,4,5], Yongqiang Liu[1,2,3,4,5], Mayibaier Maihamuti[1,2,3,4,5], Fan Yang[1,3,4,5], Chenglong Zhou[1,3,4,5], Xinghua Yang[1,3,4,5,6], Ali Mamtimin[1,3,4,5]

1.Institute of Desert Meteorology, China Meteorological Administration, Urumqi 830002, China

2.College of Geography and Remote Sensing Sciences, Xinjiang University, Urumqi 830046, China

3.National Observation and Research Station of Desert Meteorology, Taklimakan Desert of Xinjiang, Urumqi 830002, China

4.Taklimakan Desert Meteorology Field Experiment Station, China Meteorological Administration, Urumqi 830002, China

5.Xinjiang Key Laboratory of Desert Meteorology and Sandstorm, Urumqi 830002, China

6.School of Geographical Sciences, Shanxi Normal University, Taiyuan 030032, China

Corresponding Author: Wen Huo huowenpet@idm.cn ~~orcid:0000-0002-7861-2424~~

Abstract: The Taklamakan Desert (TD) is a major dust-source region in East Asia, yet the dynamic and thermal processes associated with dust-storm development remain insufficiently understood from vertically resolved observations. This study combined dual-gradient tower observations from Tazhong (TZ) and Xiaotang (XT), ERA5 reanalysis, and HYSPLIT backward trajectories to examine eight dust-storm events in spring and summer 2024. Three main pre-storm airflow pathways were identified: east-inflow transport through the northeastern Tarim Basin, mountain-crossing transport across the Tianshan–Pamir region, and south-to-north transport across the Tibetan Plateau and Kunlun Mountains. ERA5 anomaly diagnostics show that spring events maintained stronger mean sea-level pressure-gradient and 850 hPa geopotential-height-gradient anomalies throughout the pre-onset period, while 10 m wind-speed anomalies increased rapidly after approximately −12 h. In contrast, summer events showed stronger thermal signals before approximately −18 h, including enhanced surface–air temperature contrast, positive net shortwave radiation anomalies, and boundary-layer growth. Tower observations further indicate stronger summer warming and closer-to-onset wind-speed and wind-shear enhancement. Differences between TZ and XT suggest that local terrain modulates the near-surface response to regional dynamic and thermal forcing. These findings provide observational evidence for seasonal differences in TD dust-storm processes. ~~The Taklamakan Desert (TD) is a~~

设置了格式: 字体: (中文) Times New Roman, 17 磅
设置了格式: 字体: (中文) Times New Roman, 17 磅
带格式的: MS title, 左, 缩进: 首行缩进: 0 厘米
设置了格式: 字体: (中文) Times New Roman, 小四, 英语(英国)
设置了格式: 字体: (中文) Times New Roman, 小四, 英语(英国)
设置了格式: 字体: 小四
设置了格式: 字体: (中文) Times New Roman, 小四, 英语(英国)
设置了格式: 字体: 小四
设置了格式: 字体: (中文) Times New Roman, 小四, 英语(英国)
设置了格式: 字体: 小四
设置了格式: 字体: (中文) Times New Roman, 小四, 英语(英国)
设置了格式: 字体: 小四
设置了格式: 字体: (中文) Times New Roman, 小四, 英语(英国)
设置了格式: 字体: 小四
设置了格式: 字体: (中文) Times New Roman, 小四, 英语(英国)
设置了格式: 字体: 小四
设置了格式: 字体: (中文) Times New Roman, 小四, 英语(英国)
设置了格式: 字体: 小四
设置了格式: 字体: 10 磅
设置了格式: 字体: 10 磅
带格式的: 缩进: 首行缩进: 0 字符, 段落间距段前: 6 磅
带格式的: 缩进: 首行缩进: 0 字符
设置了格式: 字体: (中文) Times New Roman, 10 磅, 倾斜, 英语(英国), 非加宽量 / 紧缩量
设置了格式: 字体: 倾斜
设置了格式: 字体: (中文) Times New Roman, 英语(英国), 非加宽量 / 紧缩量
设置了格式: 字体: (中文) Times New Roman, 10 磅, 英语(英国), 图案: 清除
带格式的: 正文, 缩进: 首行缩进: 0 厘米, 段落间距段前: 6 磅, 段后: 18 磅, 图案: 清除
域代码已更改
带格式的: 缩进: 右侧: 0 厘米, 首行缩进: 0 字符

key source of dust storms in East Asia, frequently impacting China and neighboring countries. Based on dual-gradient observational experiments in the central and peripheral regions of the TD, combined with ERA5 data and HYSPLIT analysis, eight dust storms from April to June 2024 were studied. The findings include:(1)Dust storm trajectories in the TD fall into three types: (a) east-to-west movement, (b) transport across the Tianshan and Pamir Mountains, and (c) west-to-east movement driven by thermal factors in summer.(2)Spring dust storms (March–April) are dominated by dynamic factors, while summer storms (May–June) are influenced by thermal factors. Significant pressure and temperature changes 12–6 hours before a storm provide a critical prediction window.(3)Horizontal dust flux (Q) at XiaoTang (peripheral region) follows a parabolic pattern, while at TaZhong (central region), terrain plays a key role. High Q values result in larger fluctuations, while low Q values show relative stability. Seasonal temperature differences, convective intensity, and flat terrain drive alternating wind speed trends at XiaoTang before storms, with stronger fluctuations observed in summer due to rising temperatures.

设置了格式：英语(英国)

Keywords: Dust storm; Taklimakan Desert; HYSPLIT; ERA5; dynamic and thermal anomalies; vertical observationDust Storms, Backward Trajectory Analysis, Causation Analysis, Horizontal And Vertical Dust Flux Analysis

1 Introduction

带格式的：标题 1，无，缩进：首行缩进： 0 厘米，右侧： 0 厘米，段落间距段前：0 磅，段后：0 磅

Dust storms are among the major natural hazards in arid and semi-arid regions of East Asia, where they are often accompanied by strong winds, air pollution, and reduced visibility, affecting transportation, agriculture, ecosystems, and public health (Achakulwisut et al., 2018; Bao and Fang, 2007; Manisalidis et al., 2020; Shao and Dong, 2006; Tong et al., 2023; Wen et al., 2024). Mineral dust can also influence atmospheric radiation, cloud processes, snow and ice albedo, and regional climate through long-range transport (Kok et al., 2023; Prospero, 1999).

The Taklimakan Desert (TD) is located in the arid Tarim Basin and is surrounded by the Tianshan, Pamir, and Kunlun Mountains. Because of its extensive mobile sand surfaces, scarce precipitation, and unique basin topography, the TD is one of the major dust-source regions in East Asia (Ge et al., 2014; Shao and Dong, 2006; Wang et al., 2015; Xu et al., 2020; Yang et al., 2016; Zhang et al., 2025).

The formation and development of dust storms are jointly controlled by atmospheric forcing and surface conditions. Among these controls, dynamic and thermal processes are particularly important because they determine whether surface particles can be lifted and whether the lifted dust can be transported vertically and horizontally (Bi et al., 2022; Su et al., 2024; Zhang et al., 2024). Dynamic forcing, represented by pressure-gradient-driven winds, cold fronts, cyclones, and low-level jets, provides the direct momentum for dust emission (Shao and Dong, 2006; Xu et al., 2020). Thermal forcing, mainly associated with strong surface heating, boundary-layer growth, turbulent mixing, and land–atmosphere temperature contrasts, can enhance vertical exchange and promote dust uplift, especially over inland deserts with intense surface heating (Wang et al., 2025; Xiong et al., 2023). Surface factors such as particle-size distribution, soil moisture, vegetation cover, and aerodynamic roughness further regulate the threshold and intensity of dust emission (Iversen and White, 1982; Marticorena and Bergametti, 1995; Raupach, 1992; Shao and Dong, 2006). Therefore, dust-storm processes cannot be explained by a single factor alone, but should be examined through the coupled effects of dynamic forcing, thermal instability, transport pathways, and terrain-modified local surface conditions.

Previous studies have shown that dynamic forcing is a key driver of many spring dust storms in East Asia. Mongolian cyclones, cold fronts, cold high-pressure systems, and strong pressure gradients can generate strong near-surface winds and rapidly activate dust sources over Mongolia, northern China, and the Tarim Basin (Gao et al., 2024; Liu et al., 2004; Wang et al., 2009; Xu et al., 2020). S. Chen et al. (2023a) showed that severe dust events in northern China during March and April 2023 were closely related to cold fronts and Mongolian cyclones, with Mongolia and the Taklimakan Desert both contributing substantially to dust concentrations. Li et al. (2023) further demonstrated that dust radiative feedback can influence the intensity and movement of Mongolian cyclones and cold fronts, indicating that dust storms are not only a response to weather systems but may also interact with them. More recently, Mu et al. (2025) quantitatively assessed the role of atmospheric depressions and Mongolian cyclones in spring dust activity over East Asia and found that Mongolian cyclones are a key driver of high-impact dust events. These studies highlight the importance of synoptic-scale dynamic forcing in East Asian dust-storm development. However, many of them focus on northern China and the Gobi source region, whereas the pre-storm dynamic evolution over the Taklimakan Desert, especially its connection with local tower-based observations, remains less well documented.

Compared with the relatively well-recognized role of dynamic forcing, the influence of thermal forcing is more complex and is particularly important for inland desert regions such as the TD. Strong solar heating over mobile sand surfaces can increase the surface–air temperature difference, deepen the atmospheric boundary layer, enhance turbulent mixing, and create favorable conditions for vertical dust uplift (Chen et al., 2023b; Xiong et al., 2023; Yuan et al., 2019; Zhang et al., 2025). Yuan et al. (2019) investigated the influence of dynamic and thermal forcing on the meridional transport of Taklimakan dust in spring and summer and emphasized that seasonal differences in dust transport are closely linked to changes in forcing mechanisms. Y. Chen et al. (2023b) used WRF-Chem simulations to investigate the radiative effects of dust aerosols on weather conditions and dust transport over the TD. Their results suggested that dust–radiation interactions can modify temperature, wind fields, and vertical dust transport, indicating the potential importance of thermal feedbacks in dust-storm evolution. X. Zhang et al. (2025) further indicated that spring Taklimakan dust transported toward the Tibetan Plateau is controlled by circulation patterns, dynamic lifting, thermal anomalies, and terrain effects. These findings suggest that distinguishing between dynamic and thermal controls is useful for understanding seasonal differences in dust-storm development. Nevertheless, how these seasonal differences are reflected in near-surface wind, temperature, and vertical meteorological profiles still requires further observational evidence, particularly from direct comparisons between spring and summer events.

Transport pathways provide an important way to connect dynamic and thermal forcing with dust-storm evolution. They reflect not only where air masses and dust originate, but also how synoptic circulation, basin-scale airflow, and thermal lifting organize dust movement before and during dust storms. Kai and Huiwang (2007) identified major East Asian dust transport pathways toward eastern China, Korea, Japan, the western Pacific, and Central Asia. T. Bao et al. (2023) examined East Asian dust sources and transport ranges from 1980 to 2020 using ground observations and remote sensing data, and showed that southern Mongolia and the Taklimakan Desert are major source areas. For the TD, Aili et al. (2021) found that air masses during the dusty season at the northeastern desert margin mainly originated from the eastern and southern parts of the desert, indicating the importance of intra-basin transport. Aili et al. (2024) further used HYSPLIT trajectories to establish an early-warning framework for dusty weather in peri-desert regions of the TD. These studies demonstrate the value of trajectory analysis, but pathway classification alone cannot fully explain why different dust storms develop under different dynamic or thermal backgrounds.

Topography further modifies dust-storm occurrence, transport, and near-surface wind and temperature structures. The TD is enclosed by high mountains and connected to surrounding regions through limited basin openings, so airflow pathways are strongly constrained by terrain. The Tarim Basin and surrounding mountain systems can channel near-surface winds, favor dust accumulation within the basin, and promote vertical lifting under suitable dynamic and thermal conditions (Sun and Liu, 2006; Xing et al., 2024; Yuan et al., 2019; Zhang et al., 2025). Thus, topography is closely linked to both transport pathways and dynamic–thermal forcing rather than being only a static background condition. At the local scale, dune relief and underlying-surface differences can alter wind profiles, near-surface thermal structure, and sediment availability. (Aili et al., 2023).

Dust storms are one of East Asia's most severe natural disasters, occurring frequently in arid and semi-arid regions such as the Taklamakan Desert in China and the Gobi Desert bordering Mongolia. These events are widespread in spring, impacting millions(Bao & Fang, 2007; Shao & Dong, 2006). Dust storms are often accompanied by air pollution, strong winds, and significant reductions in visibility, severely affecting human life and production activities. These disasters disrupt agriculture, transportation, and infrastructure and pose threats to public health, particularly by significantly increasing the incidence of respiratory diseases(Achakulwisut et al., 2018; Manisalidis et al., 2020; Mohebbi et al., 2019; Tong et al., 2023; Wen et al., 2024).In addition, dust storms negatively impact ecosystems by causing soil degradation and water source contamination, further exacerbating the ecological vulnerability of affected regions (Ma et al., 2020; Perez et al., 2008).

Meanwhile, the frequent occurrence of dust storms may also intensify global climate change and exacerbate challenges in cross-regional environmental governance(Prospero, 1999; Zong et al., 2021). The Taklamakan Desert is in Asia's arid and semi-arid regions, characterized by scarce precipitation, vast sandy terrain, and dry climatic conditions. Combined with the influence of Mongolian cyclones, these factors make the region prone to frequent dust storms in spring, establishing it as one of the primary dust sources in East Asia (Shao & Dong, 2006; Xu et al., 2020).

The formation of dust storms is a complex physical process driven by interactions between the atmosphere and surface soil, where dust source materials, dynamic conditions, and thermal factors play critical roles in influencing their occurrence. The characteristics and quantity of dust source materials determine the generation and intensity of dust. As the dynamic condition, wind is the primary direct factor triggering dust storms, while thermal factors provide strong supportive conditions for their occurrence(Iversen & White, 1982). The formation of dust storms is also influenced by various factors related to surface dust source materials, including dust particle size, soil moisture, and vegetation cover. When soil particle size exceeds 60–70 μm, the threshold for dust emission increases gradually with particle size due to the gravitational influence of the particles themselves. Conversely, when particle size is less than 60–70 μm, the increased cohesive forces between particles significantly raise the dust emission threshold as particle size decreases (Iversen & White, 1982; Marticorena & Bergametti, 1995).In addition, soil particle size affects dust emission flux during dust storm events(Yang et al., 2016). Soil moisture is likewise a crucial influencing factor. On one hand, higher moisture levels enhance the adhesive forces between particles; conversely, they promote the aggregation of fine particles, thereby suppressing sand mobilization and reducing dust fluxes(Iversen & White, 1982; Shao & Dong, 2006). The increase in vegetation effectively suppresses the occurrence of dust storms or mitigates their intensity by reducing the supply of sand sources and dissipating wind energy(MacKinnon et al., 2004; Raupach, 1992).

In East Asia during spring, there is a significant positive correlation between strong winds and the frequency of dust storms (Xu et al., 2020).In East Asia, Mongolian cyclones frequently generate strong winds, which in turn lead to the formation of dust storms. These cyclones exhibit pronounced seasonality (March to May) and are typically accompanied by weather conditions such as strong winds, temperature drops, dust emissions, and significant reductions in visibility.Their impact is not confined to Mongolia and northern China but can extend across the entire East Asian region. Through upper-atmosphere circulation, these effects may even spread to more distant areas, such as Korea, Japan, and the western Pacific coast(Liu et al., 2004; X. Wang et al., 2009)

Horizontal and vertical dust fluxes jointly determine the spatial extent of dust dispersion, which is critical in shaping global dust transport pathways. High vertical dust fluxes can transport dust to more distant regions, thereby influencing atmospheric chemical composition, climate systems, and ecological environments. Accurately understanding dust flux is crucial for improving dust storm forecasting, particularly within climate models, as it aids in better predicting the impacts of dust on air quality and ecosystems(S. Chen et al., 2023b). Recent studies have focused on this field, revealing several significant findings. Research by (Kai & Huiwang, 2007) identified three primary transport pathways for East Asian dust storms:1) Passing through China and depositing in the Bohai Sea, Korea Strait, Sea of Japan, and Yellow Sea;2) Extending westward into Central Asia;3) Reaching as far as the western Pacific under the influence of strong northwesterly winds. Additionally, many researchers have utilized the WRF-Chem model to analyze dust emissions from different regions, thereby improving the numerical prediction of dust storms, particularly in terms of transport and deposition calculations(DeMeester & Johnson, 1975; Hosseini Dehshiri & Firoozabadi, 2024; Rizza et al., 2017; Y. Zeng et al., 2020). For the Taklamakan Desert, observational data from (Aili et al., 2023)indicate a significant decreasing trend in deposition rates across different underlying surfaces in the northeastern desert-oasis transitional zone. The order is as follows: mobile sand desert > semi mobile sand desert > desert vegetation > shelterbelt forest > farmland. This demonstrates the effectiveness of increased vegetation in suppressing dust storms. Improved WRF-Chem simulation results by (Y. Chen et al., 2023) indicate that in the Taklamakan Desert, the formation of summer dust storms is primarily influenced by thermal factors. In contrast, spring dust storms are dominated by dynamic factors.(Huo et al., 2022), based on dual gradient observational experiments in the central and peripheral regions of the desert, found that in flat areas, horizontal dust flux (Q) and vertical dust flux (F) exhibit a linear relationship and an exponential variation with height. However, no significant changes were observed over undulating terrain.(H. Wang et al., 2015), through field observations, measured the horizontal wind erosion flux and dust emissions during windblown sand/dust processes across arid and semi-arid regions in northern China. Their findings revealed that the Taklamakan Desert exhibits significantly stronger horizontal dust flux than other studied regions, thus identifying it as a significant source of dust emissions.

In summary, due to observational methods' limitations, most studies rely on remote sensing data to calculate horizontal and vertical dust fluxes (Q and F) or analyze observational data. Few studies have successfully integrated both approaches. Research that integrates multiple data sources to comprehensively analyze the variations in Q and F and the underlying driving factors is relatively scarce and remains an area for further exploration. In this context, the present study conducted dual-point gradient synchronous dust storm observational experiments in the Taklamakan Desert, obtaining multiple key parameters and their differences under various topographical conditions. It also incorporated reanalysis data and backward trajectory analysis. This approach further enhanced the ability to analyze the dynamic characteristics of dust storms. Remote sensing data strongly supports the spatial distribution and diffusion of dust storms on a large scale. At the same time, backward trajectory analysis effectively traces dust storms' origins and transport pathways. Combining multiple data sources, this approach overcomes the limitations of single observational methods and offers a more comprehensive analytical perspective.

~~Through the comprehensive analysis of these data, the study provides an in-depth understanding of how different topographical features in the Taklamakan Desert influence key parameters of dust storms. It also offers strong technical support for investigating, monitoring, and predicting dust storm formation. This deepens the understanding of dust storm characteristics and their evolution and enhances the recognition of the Taklamakan Desert's influence on dust emissions and transport in Asia and globally. This provides valuable reference points for future related research and lays a solid scientific foundation for preventing and managing dust storms.~~

~~Section 2 of this paper describes the study area, the data used, and the methodology. Section 3 analyzes dust trajectories, the meteorological background of dust storms, and their dynamic and thermal factors. It also examines the horizontal and vertical fluxes and temperature and wind speed variations across different desert topographies based on observational data. The discussion and conclusions are presented in Sections 4 and 5, respectively.~~

2 Study Area, Data, and Methodology

带格式的：标题 1，无，缩进：首行缩进： 0 厘米，右侧： 0 厘米，段落间距段前：0 磅，段后：0 磅

2.1 ~~-~~Study Area

The Taklamakan Desert (TD) is located within the Tarim Basin in the southwestern part of the Xinjiang Uyghur Autonomous Region in China. It is the second-largest shifting sand desert in the world. Surrounded by mountain ranges such as the Tianshan and Kunlun Mountains, the region experiences a highly arid climate. Key characteristics of the desert include its remoteness from the ocean, sparse vegetation, diverse dune types with high mobility, extensive and thick shifting sand areas, and fine sand particles. This region is subject to frequent dust storms year-round and is one of the significant sources of dust storms in East Asia(Sun and Liu, 2006)~~(Sun & Liu, 2006)~~.

域代码已更改

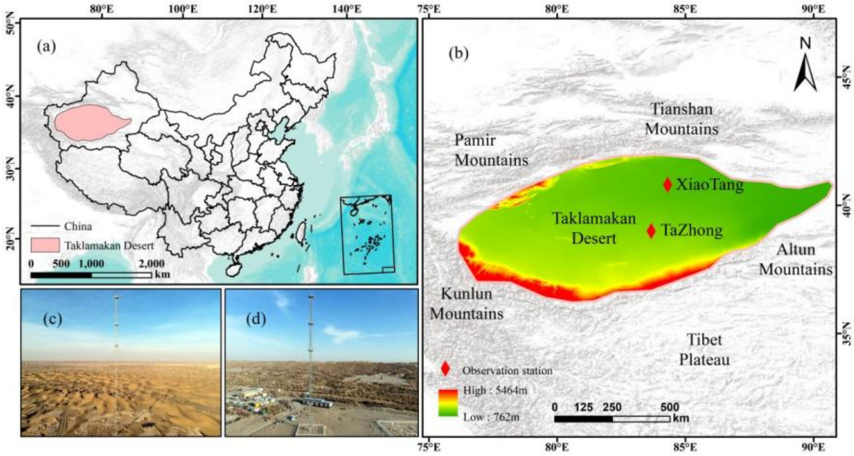

Fig. 1. Location and topography of the Taklimakan Desert, including the Tazhong (TZ) and Xiaotang (XT) observation towers and site photographs.**Fig. 1 Location and topography of the Taklimakan Desert, and the TZ and XT observation towers (maps and site photos)**

2.2 –Observational Data

The observational data were obtained from two stations: Xiaotang (XT)X Station, located on the northern edge of the TDTaklamakan Desert, representing flat terrain, and TZ Station, situated in the desert interior, representing undulating terrain. The observation tower height is 80 m at TZ and 100 m at XTTZ Station is at an elevation of 80 meters, while X Station is at 100 meters. Both stations are equipped with meteorological gradient observation systems and dust collection systems. The observation levels at TZgradient layers at TZ Station are at 1 m, 2 m, 5 m, 8 m, 16 m, 24 m, 32 m, 47 m, 63 m, and 80 m. while those at XT are 1 m, 2 m, 5 m, 10 m, 24 m, 32 m, 47 m, 63 m, 80 m, and 100 m.At XT Station, they are at 1 m, 2 m, 5 m, 10 m, 24 m, 32 m, 47 m, 63 m, 80 m, and 100 m.

The meteorological gradient observation system records meteorological variablesclimate parameters at each layer, including hourly and minute-based measurements of temperature, relative humidity, wind speed, wind direction, and atmospheric pressure. The dust collection system gathers dust samples during dust storms using BSNE dust collectors installed at each layer. In the present analysis, the meteorological gradient observations were mainly used to examine wind-speed, wind-shear, and temperature-profile responses during dust-storm development.The gradient collection system gathers dust samples during dust storms using BSNE (Big Spring Number Eight) dust collectors installed at each layer, which are used to determine the horizontal dust flux at different heights.

带格式的：缩进：首行缩进： 0 字符

设置了格式：字体：非加粗

带格式的：题目，左，缩进：首行缩进： 0 厘米

带格式的：标题 2，无，缩进：左侧： 0 厘米，悬挂缩进：4.02 字符，段落间距段前：0 磅，段后：0 磅，制表位：不在 3.6 字符

Nine dust storm events were observed between 31 March and 18 June 2024~~April 3 and July 10, 2024~~, and the corresponding dust samples were collected from 3 April to 10 July 2024 (as detailed in Table 1). However, during the second observation, data from ~~the~~ TZ~~TZ Station~~ were missing, preventing a complete paired record. Therefore, the remaining eight complete dust storm events observations became the primary samples for this study.~~Therefore, the remaining eight observations became the primary samples for this study.~~

To reduce the influence of seasonal variation and diurnal cycles on the station-based meteorological profiles, a background-removal procedure was applied to the observational data from both TZ and XT. For each dust-storm event, observation height, and variable, the background value was calculated separately for the two stations using records from 2023 and 2025. Specifically, for a given observation time in 2024, all available records at the same hour of the day within a ±15-day calendar window in 2023 and 2025 were averaged to represent the corresponding background state. The anomaly was then obtained by subtracting this station-specific background value from the observed value during the 2024 dust-storm process. This approach reduces the effects of normal seasonal progression and daily temperature or wind-speed cycles, allowing the analysis to focus on meteorological anomalies directly associated with dust-storm development.

Table~~Tab.~~ 1. Summary of observed dust-storm events and sample collection information~~Sample details~~

Event ID	Station ~~Name~~	Start time of dust storm	Duration (h)~~Duration time(h)~~	Sample collection time
Dust1	TZ	2024-03-31 12:00~~2024.3.31~~	22	2024-04-01 09:00~~2024.4.3~~
	XT	2024-03-31 12:40~~2024.3.31~~	17.3	2024-04-01 06:00~~2024.4.4~~
Excluded event ~~2~~	XT	2024-04-05 01:00~~2024.4.5~~	5	2024-04-05 06:00~~2024.4.6~~
Dust~~3~~2	XT	2024-04-12 04:00~~2024.4.12~~	7.5	2024-04-12 14:00~~2024.4.16~~
	TZ~~(~~	2024-04-14 04:00~~2024.4.12~~	11	2024-04-14 15:00~~2024.4.15~~
Dust~~4~~3	XT~~TZ~~	2024-04-17 11:00~~2024.4.17~~	23	2024-04-18 10:00~~2024.4.20~~
	~~XT~~TZ	2024-04-18 10:00~~2024.4.17~~	36	2024-04-19 22:00~~2024.4.21~~
Dust~~5~~4	TZ	2024-04-26 21:00~~2024.4.26~~	16.5	2024-04-27 13:30~~2024.5.12~~

带格式的：两端对齐

格式化表格

设置了格式：字体：（中文）宋体，六号，字体颜色：黑色

设置了格式：字体颜色：黑色

设置了格式：字体：（中文）宋体，六号，字体颜色：黑色

	XT	2024-04-26 02:00~~2024.4.26~~	~~42.5~~31	2024-04-27 09:00~~2024.5.12~~
Dust~~6~~5	TZ	2024-05-12 07:00~~2024.5.12~~	24	2024-05-12 14:30~~2024.5.16~~
	XT	2024-05-12 07:30~~2024.5.12~~	~~55~~7	2024-05-12 14:30~~2024.5.17~~
Dust~~7~~6	TZ	2024-05-20 11:00~~2024.5.20~~	~~40~~14	2024-05-20 14:30~~2024.6.3~~
	XT	2024-05-20 11:00~~2024.5.20~~	~~27.5~~3.5	2024-05-20 14:30~~2024.5.30~~
Dust~~8~~7	TZ	2024-06-04 04:00~~2024.6.4~~	12	2024-06-04 16:00~~2024.6.10~~
	XT	2024-06-04 04:00~~2024.6.4~~	3~~7~~	2024-06-04 07:00~~2024.6.10~~
Dust~~9~~8	TZ	2024-06-18 07:00~~2024.6.18~~	~~58~~2	2024-06-18 09:00~~2024.7.9~~
	XT~~)~~	2024-06-18 07:20~~2024.6.18~~	~~22~~3.7	2024-06-18 11:00~~2024.7.10~~

2.3 ERA5 Reanalysis Data ~~Remote Sensing Data~~

To further investigate the meteorological conditions associated with dust storm occurrence~~causes of dust storms~~, this study used the ERA5 reanalysis dataset. ~~the study analyzed relevant meteorological conditions using the ERA5 reanalysis dataset.~~ ERA5, provided by the European Centre for Medium-Range Weather Forecasts (ECMWF), is the fifth generation of global atmospheric~~climate and weather~~ reanalysis data. It has a spatial resolution of 0.25° × 0.25° and a temporal resolution of 1 hour.

In this study, ERA5 data were used in two ways. First, the original ERA5 fields were used to describe the synoptic-scale meteorological background before and during each dust-storm event, including mean sea-level pressure, 10 m wind vectors, 2 m air temperature, and 850 hPa geopotential height. These fields were mainly displayed over the regional domain of 70–100° E and 30–50° N to identify the pressure configuration, airflow pathway, and thermal background around the Taklamakan Desert.

Second, selected ERA5-derived diagnostic indicators were used for anomaly analysis after background removal. The dynamic indicators included mean sea-level pressure-gradient magnitude, 850 hPa geopotential-height-gradient magnitude, and 10 m wind speed. These indicators were averaged over the regional domain of 70–100° E and 30–50° N to represent the large-scale dynamic background around the TD and its surrounding mountains. The thermal indicators included 2 m air temperature, skin temperature, surface–air temperature difference, surface net shortwave radiation, and boundary-layer height. These indicators were averaged over the Taklamakan Desert core region. The desert core was defined using a Taklamakan Desert polygon mask within 72–92° E and 35–43° N. Grid cells outside the

带格式的：标题 2，无，缩进：左侧： 0 厘米，悬挂缩进：4.02 字符，段落间距段前：0 磅，段后：0 磅，制表位：不在 3.6 字符

desert mask were excluded from the thermal averaging.

For each dust-storm event and each lead time relative to storm onset, the corresponding 2024 ERA5 value was extracted. The background value was calculated from ERA5 records during 2015–2025, excluding 2024, using the same hour of the day within a ±3-day calendar window. The anomaly was then obtained by subtracting this background value from the corresponding 2024 event value. Area-mean values were calculated using latitude-weighted averaging with cos(latitude) as the weight. This treatment reduced the influence of seasonal progression, diurnal variation, and unequal grid-cell area, thereby highlighting the dynamic and thermal departures related to dust-storm development.

The ERA5 reanalysis dataset has demonstrated high accuracy in East Asia and desert regions. (Y. Wang et al., 2023)compared observational meteorological parameters from the Gurbantünggüt Desert with ERA5, MERRA2, JRA-55, and NCEP-FNL data and found that ERA5 had the most minor error. To assess their reliability and accuracy, (Y. Wang et al., 2023)compared reanalysis data from NCEP/NCAR, NCEP/DOE, NCEP/CFSR, JRA-25, ERA-Interim, and MERRA (with observational data. The results showed that the mean values of geopotential height and temperature from these reanalysis datasets were generally consistent with the observational data. However, regarding specific humidity, the performance of NCEP/NCAR, NCEP/DOE, and NCEP/CFSR was inferior to that of the JRA-25, ERA-Interim, and MERRA products.

2.4 HYSPLIT ModelHYSPIT model

带格式的：标题 2，无，缩进：左侧： 0 厘米，悬挂缩进：4.02 字符，段落间距段前：0 磅，段后：0 磅，制表位：不在 3.6 字符

The study used the Hybrid Single-Particle Lagrangian Integrated Trajectory (HYSPLIT) model to analyze the transport pathways of each dust storm event. This model usesutilizes grid data from the Global Data Assimilation System (GDAS) dataset to compute backward trajectories (Stein et al., 2015)(Stein et al., 2015). The GDAS1 data have a horizontal resolution of 1° × 1° and a temporal interval of 3 h. Model vertical velocity was used for the vertical motion calculation.

For each event, backward trajectories were initialized at the dust-storm onset time. The trajectory endpoint was set at 39.43° N, 85.97° E, corresponding to the observation region used in this study. Three starting heights, 100, 500, and 1500 m above ground level (AGL), were selected to represent airflow transport at different lower-tropospheric levels. Each trajectory was traced backward for 48 h. The trajectory ending times were 12:00 UTC on 31 March, 04:00 UTC on 12 April, 11:00 UTC on 17 April, 21:00 UTC on 26 April, 07:00 UTC on 12 May, 11:00 UTC on 20 May, 04:00 UTC on 4 June, and 07:00

UTC on 18 June 2024 for Dust1–Dust8, respectively.

The method assumes that the trajectory of a particle moving within the wind field is calculated by integrating its position changes over time and space~~the integral of the particle's changes over time and space~~, with its vector velocity determined by linear interpolation in both space and time. The first-guess position~~final position~~ of the air mass is calculated using the following equation:

$$P_1(t+\Delta t) = P(t) + V(P,t)\Delta t$$

The corrected position is then calculated as:

带格式的：两端对齐，缩进：首行缩进： 2 字符

$$P(t+\Delta t) = P(t) + 0.5[V(P,t) + V(P_1, t+\Delta t)]\Delta t$$

In this equation, P represents the initial position, P_1 is the first guessed position, Δt is the time interval, and V is the velocity of the air mass or particle. The simulation was conducted online using the HYSPLIT platform provided by NOAA.~~can be conducted online .~~

~~at the following link: https://www.ready.noaa.gov/HYSPLIT_traj.php~~

The resulting trajectories were used to characterize the main pre-storm airflow histories reaching the observation region and to support the interpretation of airflow transport pathways together with ERA5 10 m wind fields.

~~2.5 The calculation of horizontal dust flux (Q) and vertical dust flux (F)~~

带格式的：标题 2，无，缩进：左侧： 0 厘米，悬挂缩进：4.02 字符，段落间距段前：0 磅，段后：0 磅，制表位：不在 3.6 字符

~~There are two primary methods for obtaining Q: the first is direct measurement in the field using various dust collection instruments; the second involves wind tunnel simulation experiments, where empirical equations are established between Q and wind speed u or friction velocity u*, and Q is then inferred based on observed u or u* values. In this experiment, direct measurement was employed. Professional personnel were hired to check the BSNE dust collectors daily to ensure they were clean and dust-free. After each dust storm, dust samples were collected and weighed on site.~~ ~~$c =$~~

~~Both domestic and international dust mobilization experiments commonly use the two-layer dust concentration gradient method to calculate F(Gillette & Passi, 1988; X. Zeng & Dickinson, 1998; Zhang et al., 2017). The formula is as follows:~~

~~$F = k$~~

~~In the formula, F represents the vertical dust flux (kg/m²/s); z_1 and z_2 are the measurement heights~~

~~(m); u* is the friction velocity (cm/s); c_1 and c_2 are the dust concentrations at the two heights (kg/m³); and k is a constant (0.4). The dust concentration ccc can be obtained by converting the dust transport data measured by the dust collectors:~~

$$c =$$

~~In the formula, c represents the dust concentration at the measurement height (kg/m³/s); M is the dust mass collected by the BSNE dust collector at the measurement height (kg); u is the average wind speed during the sampling period at the measurement height (m/s); t is the sampling time (s); and A is the inlet area of the BSNE dust collector (m²).~~

~~The formula for calculating friction velocity is as follows:~~

$$u(z) = ln$$

~~In the formula, u represents the wind speed at the observation height (cm/s); u* is the friction velocity (cm/s); z is the observation height (cm); z_0 is the surface roughness length (cm); and k is a constant (0.4).~~

3 Results and Analysis

带格式的：标题 1，无，缩进：首行缩进： 0 厘米，右侧： 0 厘米，段落间距段前：0 磅，段后：0 磅

3.1 Dust Storm Trajectory Analysis

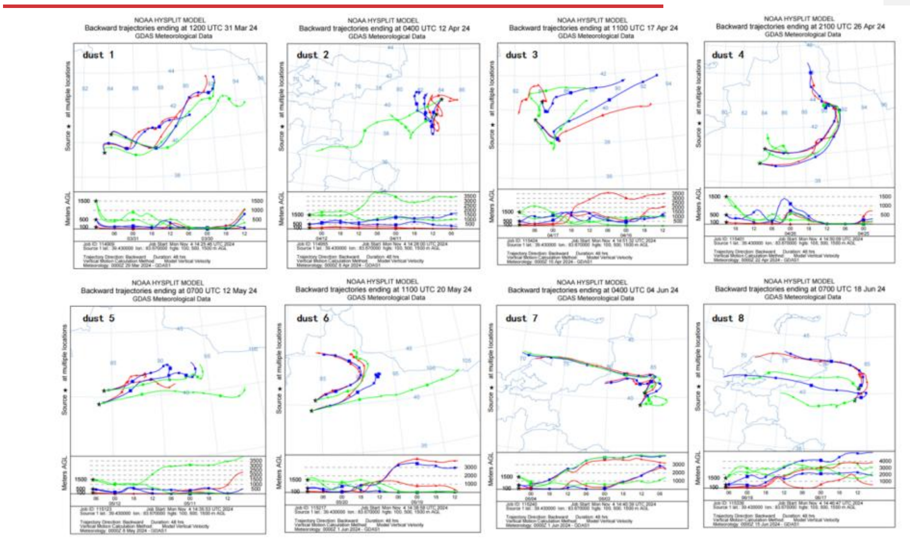

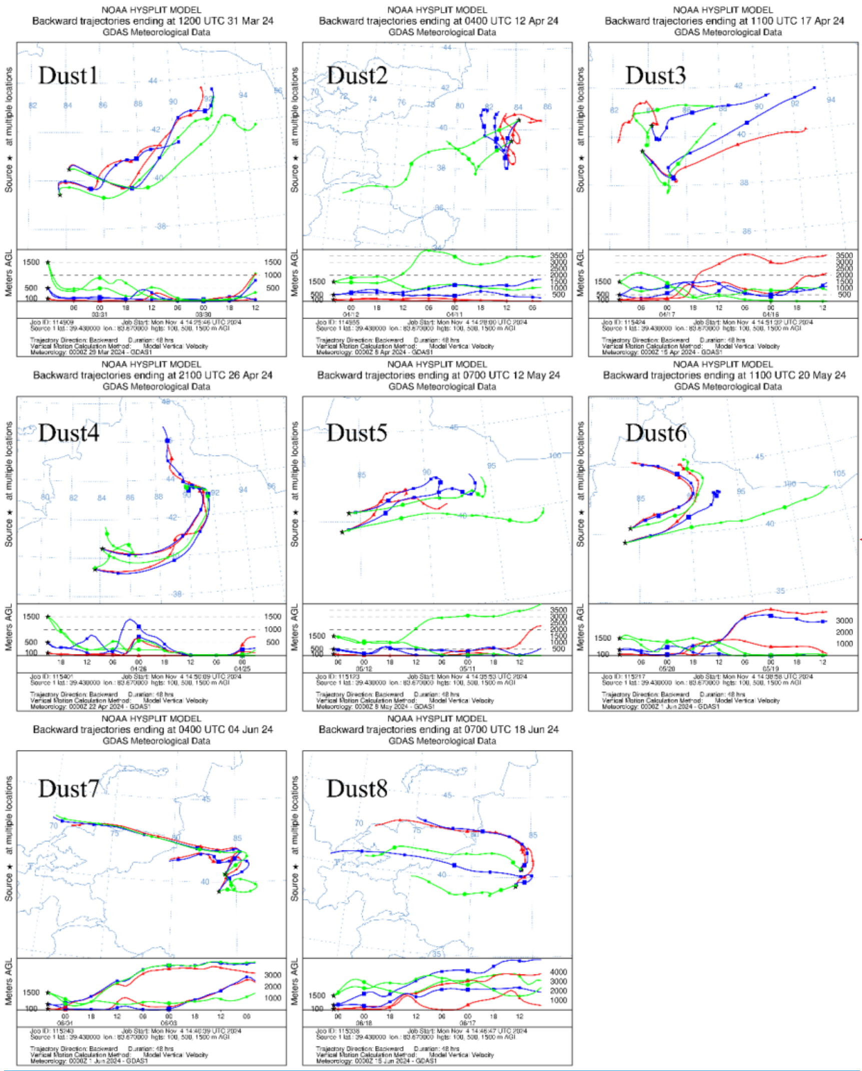

Fig. 2. Backward trajectories of the eight dust-storm events.~~**Fig. 2 Schematic diagram of the backward trajectory of these dust storms**~~

带格式的：缩进：首行缩进： 0 字符

设置了格式：字体：非加粗

带格式的：题目，左，缩进：首行缩进： 0 厘米

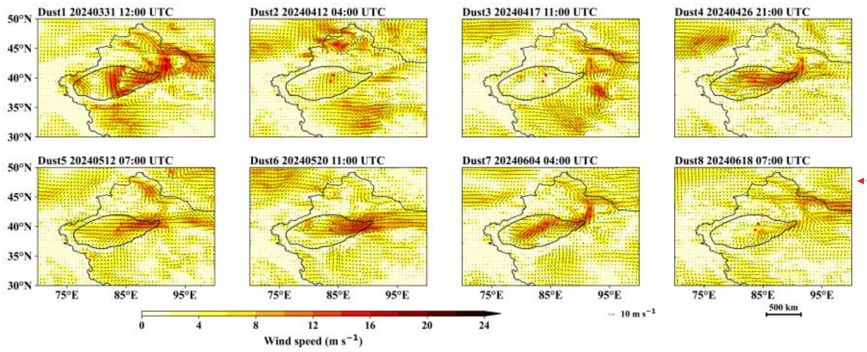

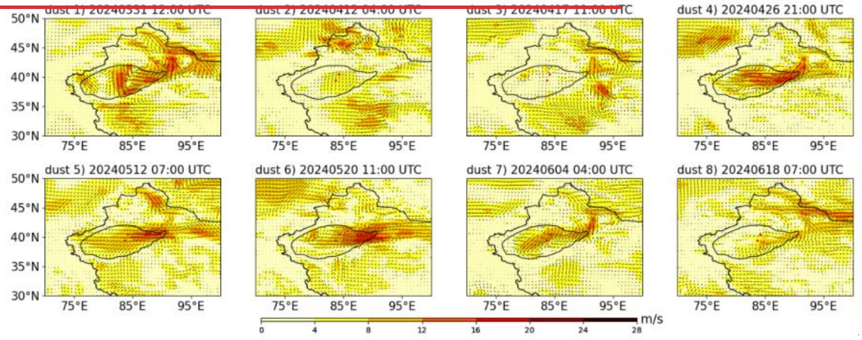

Fig. 3. ERA5 10 m wind-vector fields during the eight dust-storm events.~~**Fig. 3 10m wind vector plume field diagram**~~

As shown in Fig. 2, the HYSPLIT backward trajectories indicate that the analyzed dust-storm events were associated with three main types of pre-storm airflow transport pathways. Dust1, Dust3, Dust4, Dust5, and Dust6 mainly showed east-inflow transport, with air masses entering the TD through the northeastern opening of the Tarim Basin. Dust2 was characterized by a south-to-north pathway related to airflow crossing the Tibetan Plateau and Kunlun Mountains. Dust7 and Dust8 were associated with northwestern transport, with air masses passing over southern Russia and eastern Uzbekistan before crossing the Tianshan Mountains toward the TD.

The ERA5 10 m wind fields provide regional support for the trajectory results (Fig. 3). For most east-inflow events, the near-surface wind field shows organized airflow entering the basin through the eastern or northeastern opening. For Dust7 and Dust8, part of the airflow shows a north-to-south component, consistent with mountain-crossing transport across the Tianshan Mountains. Dust2 differs from the other events, with southerly airflow from the Tibetan Plateau toward southern Xinjiang. These results suggest that the TD dust-storm events were influenced by multiple airflow pathways, among

带格式的: 缩进：首行缩进： 0 字符

设置了格式: 字体：非加粗

带格式的: 题目，左，缩进：首行缩进： 0 厘米

which east-inflow transport was the most frequent in the analyzed cases.

As shown in Figure 2, the eight dust storm events are labeled Dust1 through Dust8, and backward trajectory simulations were conducted using the HYSPLIT model. The results show that the dust trajectories can be classified into three types: Dust1, Dust3, Dust4, Dust5, and Dust6 move from east to west, passing through a gap in the northeastern Tarim Basin before entering the desert; Dust2 originates from the Indian subcontinent, crossing the Tibetan Plateau to enter the desert; Dust7 and Dust8 are from airflow originating in southern Russia and eastern Uzbekistan, and after long-distance transport, they cross the Tianshan Mountains before reaching the desert.

The TD covers the surface with loose materials such as gravel, and strong winds carry large dust particles. The anomalous variation in wind speed is closely related to the occurrence of dust storms. Therefore, wind speed anomaly trajectories can reflect the transport paths of dust storms. Using the 10m wind components u and v from ERA5's "single-level hourly data since 1940," wind field maps were generated (Fig. 3). The figure shows that for Dust1, Dust4, Dust5, Dust6, Dust7, and Dust8, strong winds primarily enter the desert through a gap on the eastern side of the Tarim Basin, with Dust1, Dust4, Dust5, and Dust6 experiencing powerful winds. Some strong winds in Dust1, Dust3, Dust4, Dust6, Dust7, and Dust8 exhibit a north-to-south trend, crossing the Tianshan Mountains. In contrast, the strong winds, Dust2, blow from south to north from Tibet towards southern Xinjiang, consistent with the results from the backward trajectory model.

In summary, the backward trajectory analysis conducted using the HYSPLIT model based on the observation station coordinates effectively reveals the dust source trajectories passing through the stations before the occurrence of dust storms. However, it cannot fully reflect the direction of wind and its sources across the desert region. In contrast, ERA5 reanalysis data reveal the anomalous wind speeds corresponding to the HYSPLIT model and provide wind speed information for the Tarim Basin region, offering more comprehensive data for dust trajectory analysis. Based on the combined analysis of both datasets, the conclusion can be drawn that the dust storm trajectories in the TD are complex, with no single directional input, but rather a composite result of multiple directions. Most dust trajectories move from east to west, entering the desert through a gap on the eastern side of the Tarim Basin. The subsequent most common trajectories involve dust moving from north to south over the Tianshan Mountains. In contrast, fewer trajectories are observed moving from south to north across the Tibetan Plateau and over the Kunlun Mountains.

3.2 Dust Storm Dynamic and Thermal Meteorological Background

Figure 4 shows the regional mean sea-level pressure, 850 hPa geopotential height, and 10 m wind vectors before the analyzed dust-storm events. In the spring cases, especially Dust1, Dust3, and Dust4, clearer pressure differences appear between northern Xinjiang, surrounding high-pressure regions, and the TD. These pressure and circulation patterns are consistent with the east-inflow and mountain-crossing pathways identified from the trajectory analysis. Dust2 shows a different circulation background, with more evident influence from the southern and southwestern margins of the basin, corresponding to its south-to-north transport pathway.

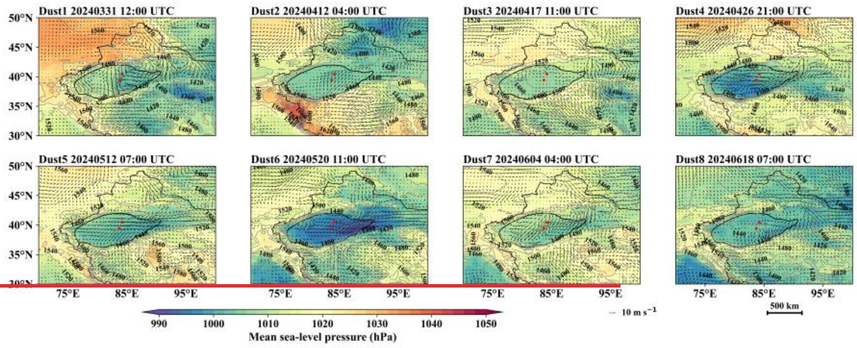

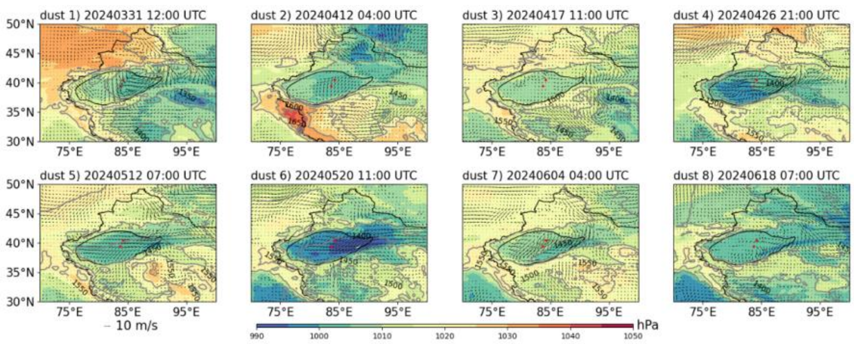

Fig. 4. Mean sea-level pressure, 10 m wind vectors, and 850 hPa geopotential height before the analyzed dust-storm events.~~**Fig.4 Mean sea level pressure, 10m wind vector, 850Phm altitude field**~~

带格式的：段落间距段后：0 磅

设置了格式：字体：(中文) +中文正文 (宋体)

带格式的：缩进：首行缩进：0 字符

设置了格式：字体：非加粗

带格式的：题目，左，缩进：首行缩进：0 厘米

设置了格式：字体：10 磅，非加粗

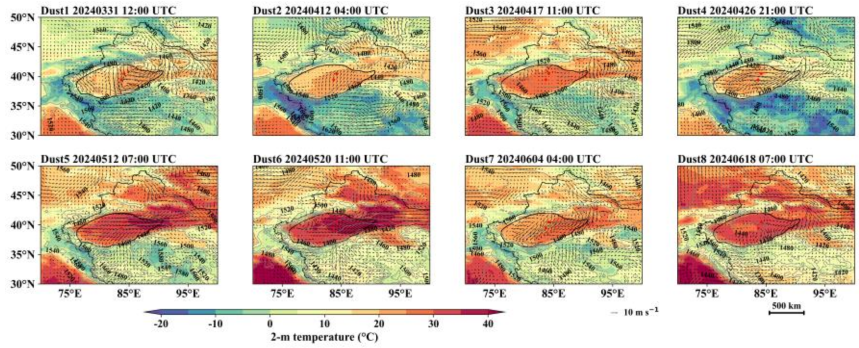

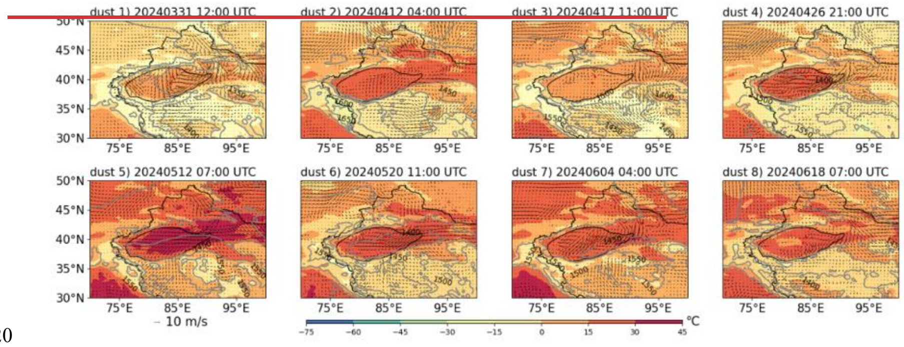

Fig. 5. 2 m air temperature, 10 m wind vectors, and 850 hPa geopotential height during the analyzed dust-storm events.~~**Fig.5** 2m temperature, 10m wind vector, 850Phm altitude field~~

In the summer cases, especially Dust7 and Dust8, the pressure-gradient signal is weaker and the dominant wind direction is less clear from the pressure field alone. This indicates that dynamic forcing was less spatially organized than in the spring cases. At the same time, Fig. 5 shows that 2 m air temperature over the TD was higher and more spatially continuous in the May–June events. Stronger surface heating may have enhanced the surface–air temperature difference, promoted boundary-layer development, and provided favorable thermal conditions for dust mobilization.

These background fields indicate a seasonal contrast in the pre-storm environment. The March–April events were more closely associated with stronger pressure-gradient and lower-tropospheric circulation signals, whereas the May–June events showed a more evident thermal background. Therefore, the analyzed events were grouped into spring cases and summer cases for the following dynamic and thermal anomaly analysis.

~~Figure 4 shows the average sea-level pressure (hPa), 850 hPa geopotential height (m), and 10 m horizontal wind (m·s⁻¹) for the periods leading up to Dust1–8. In all eight events, the north, west, and southwest regions of the Taklamakan Desert (TD) exhibited higher-than-average sea-level pressure and~~

带格式的：缩进：首行缩进： 0 字符

设置了格式：字体：非加粗

带格式的：题目，左，缩进：首行缩进： 0 厘米

geopotential height than the TD area. In the cases of Dust1, Dust3, Dust4, Dust5, and Dust6, there was a significant pressure difference between eastern Kazakhstan, southern Russia, northern Xinjiang, and the Taklamakan Desert (TD) region. This pressure gradient caused most airflow trajectories to enter the TD through the gap in the eastern Tianshan Mountains. However, some airflows crossed the western and central Tianshan Mountains before reaching the desert. For Dust2, the average sea-level pressure in the southwestern region, near the northern border of Pakistan and northern India, was 1050 hPa, with a geopotential height of 1065 m. In contrast, the pressure in the Tarim Basin region was between 1000 and 1010 hPa, with a geopotential height of 1450 m. This climatic background led to strong upper-level winds crossing the Pamir and Kunlun Mountains, ultimately entering the Taklamakan Desert (TD). In the cases of Dust7 and Dust8, the pressure gradient in the TD regionwas not as significant as in the surrounding areas, and it was not easy to indicate the direction of the strong winds. Additionally, all three dust storms occurred around noon local time during the summer. It is hypothesized that the temperature difference between the land and the atmosphere caused warm air to rise, prompting the surrounding air to flow toward the TD, generating strong winds and triggering dust storms.

Fig.5 shows the 2m temperature (°C), 850 hPa geopotential height (m), and 10 m horizontal wind ($m \cdot s^{-1}$) during the 8 dust storm events. Dust1-8 shows that the surface temperature in the Taklamakan Desert (TD) consistently exhibits high and evenly distributed temperatures. However, for Dust5, Dust7, and Dust8, the temperature in the TD region is notably higher than in other events. This increase in temperature can be attributed to the onset of May, which led to higher surface temperatures. Additionally, these three events occurred around noon, when solar radiation is strongest. The desert surface's higher specific heat capacity than the air resulted in a temperature difference between the surface and the atmosphere, creating an unstable atmospheric condition. This instability led to atmospheric convection, which generated strong winds and triggered dust storms.

In summary, the pressure gradient before dust storms in March and April is significantly greater than in May and June, while the surface temperature shows a marked increase from April to May. Therefore, dust storms occurring from March to June were categorized into two periods for analysis: spring (March and April) and summer (May and June).

3.3 Analysis of Dynamic and Thermodynamic Factors

带格式的: 标题 2, 无, 缩进: 左侧: 0 厘米, 悬挂缩进: 4.02 字符, 段落间距段前: 0 磅, 段后: 0 磅, 制表位: 不在 3.6 字符

Figures 6 and 7 show the sea-level pressure differences at 24, 12, 6, and 3 h before dust-storm onset in spring and summer, respectively. The pressure difference was calculated as the sea-level pressure at onset minus that at each preceding time. Positive values indicate pressure increase toward onset, whereas negative values indicate pressure decrease.

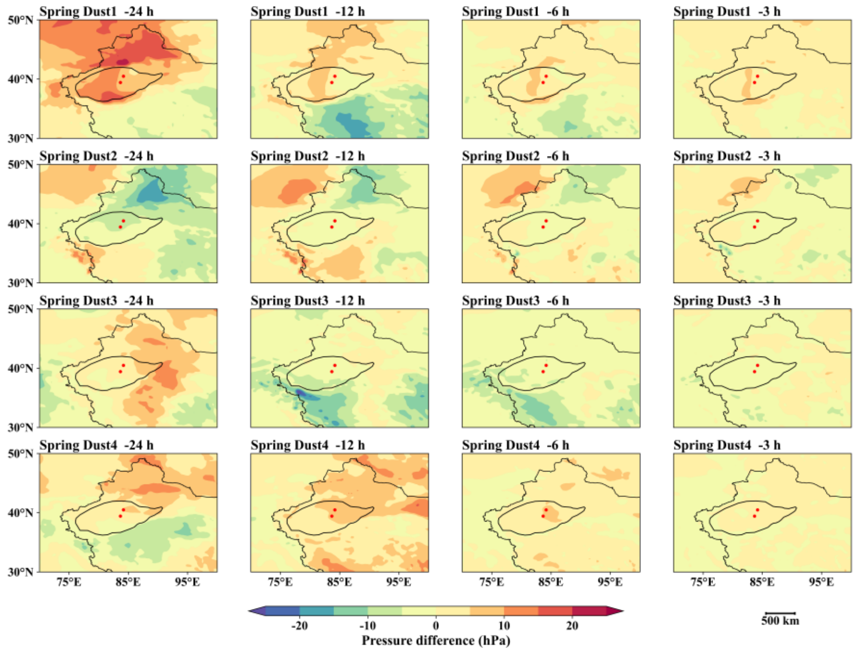

Fig. 6. Sea-level pressure differences before spring dust-storm onset.

设置了格式：字体：（中文）黑体，非加粗

带格式的：题目，缩进：首行缩进： 0 厘米，制表位：不在 3.6 字符

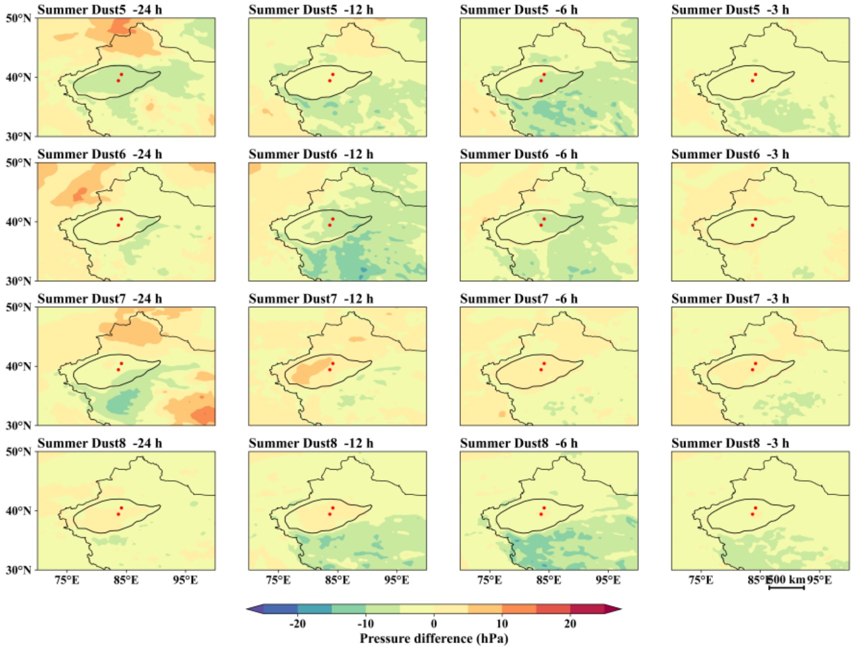

Fig. 7. Sea-level pressure differences before summer dust-storm onset.

In spring, the pressure-difference fields show stronger and more continuous spatial contrasts than in summer. For Dust1, Dust3, and Dust4, evident pressure changes appear around northern Xinjiang, the northern TD, or the eastern basin margin, indicating that the pressure-gradient system had already adjusted before onset. This agrees with the large-scale dynamic background described above, in which stronger pressure gradients and 850-hPa circulation differences favored airflows entering the TD through the eastern basin gap or crossing the Tianshan Mountains. Dust2 differs from the other spring cases, with more evident pressure changes along the southern and southwestern margins of the TD, corresponding to its south-to-north transport pathway across the plateau and mountain regions.

In summer, the pressure-difference fields are generally weaker and less spatially organized. Dust5 and Dust6 still show moderate pressure changes near the eastern or northeastern TD, consistent with their partial east-inflow characteristics. However, Dust7 and Dust8 show scattered and weak pressure-difference signals, suggesting that pressure-gradient forcing alone cannot explain their occurrence. This is consistent with the previous trajectory and background-field analysis, which indicated that summer dust storms were more likely affected by local thermal adjustment and boundary-layer development.

Figures 8 and 9 show the changes in surface–air temperature difference before dust-storm onset.

带格式的：缩进：首行缩进： 0 字符

设置了格式：字体：(中文) 黑体，非加粗

带格式的：题目，无，缩进：首行缩进： 0 厘米，段落间距段前：0 磅，段后：0 磅，制表位：不在 3.6 字符

设置了格式：字体：非加粗

The surface–air temperature difference was defined as $T_s - T_{2m}$, and its change was calculated as the onset value minus the value at 24, 12, 6, and 3 h before onset. Thus, positive values indicate that the surface–air thermal contrast strengthened toward onset, while negative values indicate that the contrast weakened.

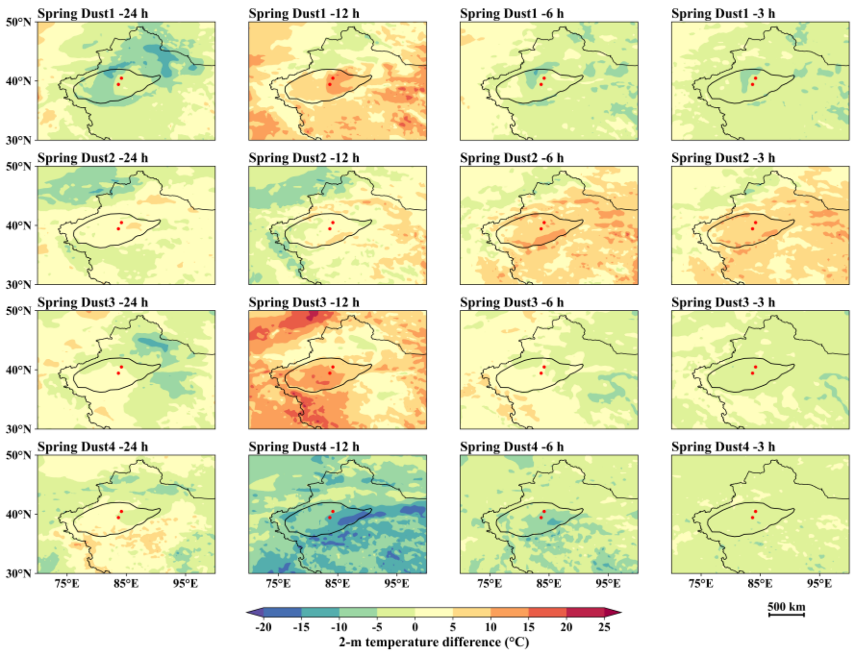

Fig. 8. Changes in surface–air temperature difference before spring dust-storm onset.

设置了格式：字体：非加粗

带格式的：缩进：首行缩进： 0 字符

设置了格式：字体：（中文）黑体，非加粗

带格式的：题目，缩进：首行缩进： 0 厘米，制表位：不在 3.6 字符

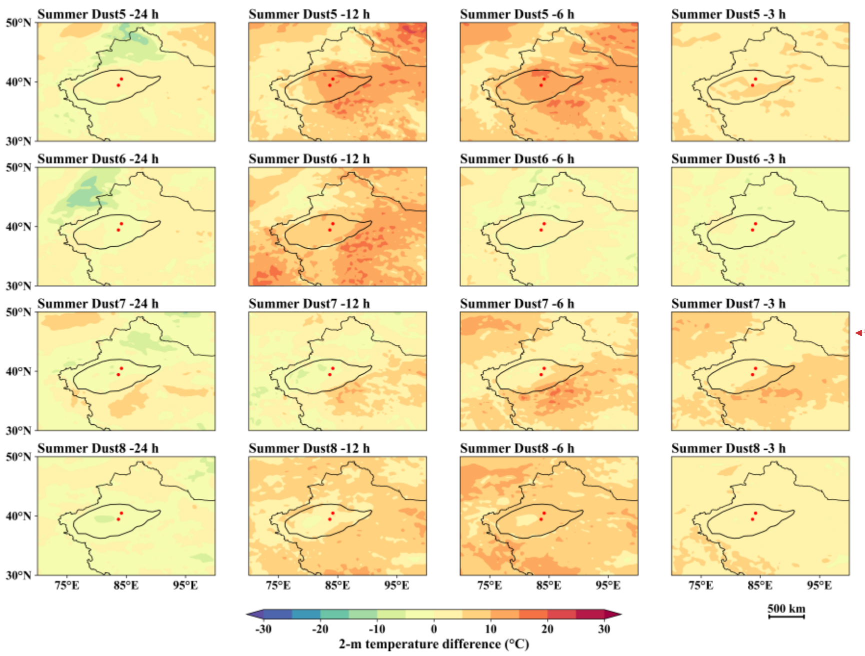

Fig. 9. Changes in surface–air temperature difference before summer dust-storm onset.

In spring, the changes in surface–air temperature difference are relatively irregular. Dust1 shows a localized increase in the thermal contrast at -12 h, but the signal weakens later. Dust2 presents a clearer increase near the southern TD, which may be related to its plateau-crossing pathway and local thermal instability. Dust3 and Dust4 show mixed positive and negative areas, indicating that the near-surface thermal structure was not consistently strengthened before all spring events. This suggests that thermal contrast may have contributed to individual spring cases, but it was not the common dominant pre-onset signal.

In summer, the increase in surface–air temperature difference is more evident. Dust5 and Dust6 show positive changes over the TD or its surrounding regions during -12 to -6 h, while Dust7 and Dust8 show broader positive areas closer to onset. These results indicate that, compared with spring, the summer cases experienced a stronger enhancement of surface–air thermal contrast before dust-storm occurrence. This pattern is consistent with the large-scale thermal background discussed above, in which stronger surface heating in May and June favored unstable stratification, turbulent mixing, and boundary-layer development.

Figure 10 further compares the composite evolution of dynamic and thermal anomalies from -24 to

带格式的：缩进：首行缩进： 0 字符

设置了格式：字体：(中文) 黑体，非加粗

设置了格式：字体：(中文) 黑体

带格式的：题目，无，缩进：首行缩进： 0 厘米，段落间距段前：0 磅，段后：0 磅，制表位：不在 3.6 字符

设置了格式：字体：非加粗

+3 h relative to dust-storm onset. The dynamic indicators are consistent with the spatial pressure-difference maps. The mean sea-level pressure-gradient anomaly and 850-hPa height-gradient anomaly remain higher in spring throughout the pre-onset period, indicating a persistent dynamic background. The 10-m wind-speed anomaly increases more sharply near onset, especially after about -12 h, suggesting that the earlier pressure-gradient adjustment was gradually transferred to near-surface wind enhancement.

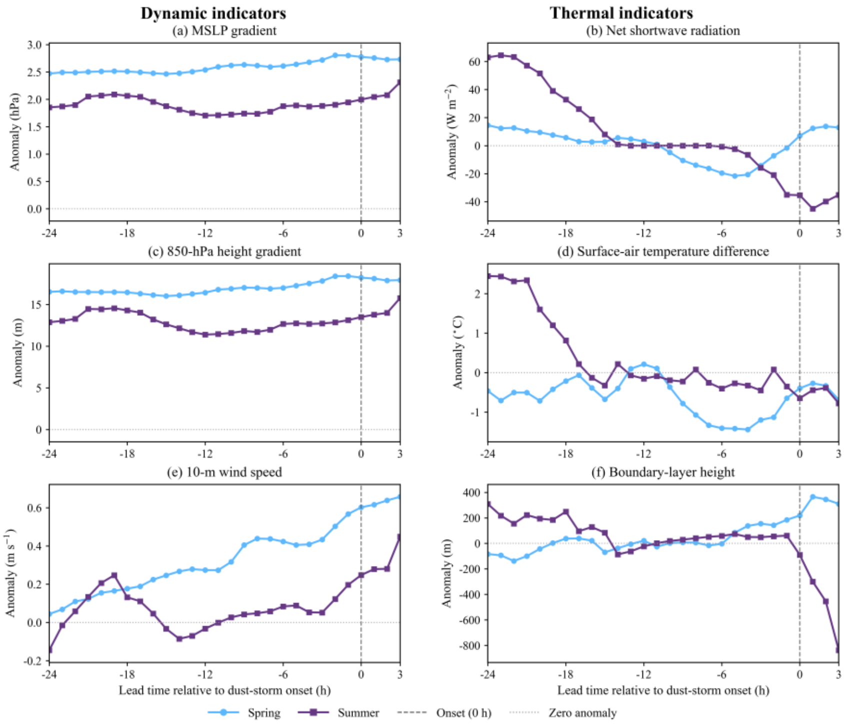

Fig. 10. Composite evolution of dynamic and thermal anomalies from −24 to +3 h relative to dust-storm onset.

The thermal curves support the spatial characteristics shown in the surface–air temperature-difference maps. In summer, the net shortwave-radiation anomaly is strongly positive during the early pre-onset stage, and the surface–air temperature-difference anomaly is also positive before about -18 h. Meanwhile, the boundary-layer-height anomaly reaches approximately 200–300 m, indicating that stronger radiation and surface heating promoted boundary-layer growth before summer dust storms. After about -12 h, the summer thermal anomalies weaken, while the near-surface wind anomaly begins to increase. This suggests that summer thermal forcing mainly provided early preconditioning, and the final onset still required near-surface wind enhancement.

带格式的： 缩进：首行缩进： 0 字符

设置了格式： 字体：(中文) 黑体，非加粗

带格式的： 题目，缩进：首行缩进： 0 厘米，制表位：不在 3.6 字符

设置了格式： 字体：非加粗

带格式的： 无，缩进：首行缩进： 2 字符，段落间距段前：0 磅，段后：0 磅

Overall, the spring dust storms were more closely linked to persistent dynamic forcing, including pressure-gradient adjustment, 850-hPa circulation differences, and subsequent wind enhancement. These features correspond well to the east-inflow and mountain-crossing pathways. In contrast, the summer cases showed weaker pressure signals but stronger early thermal preconditioning, expressed as enhanced surface–air temperature contrast, positive radiation anomalies, and boundary-layer growth. Therefore, the seasonal difference reflects a shift from dynamic-dominated spring processes to thermally preconditioned summer processes, rather than a complete separation between dynamic and thermal mechanisms.

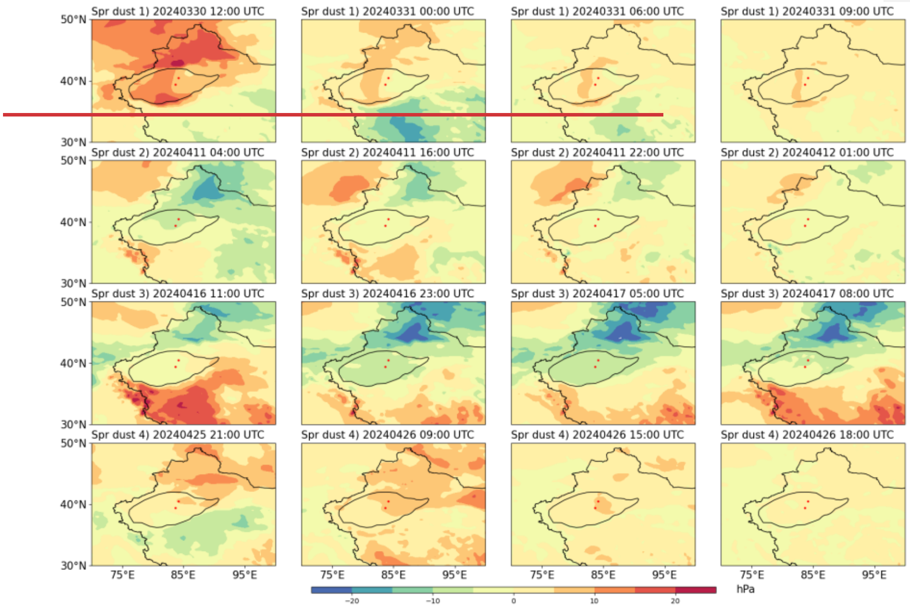

~~Fig.6 Spring sandstormΔ24h,Δ12h,Δ6h,Δ3h pressure difference~~

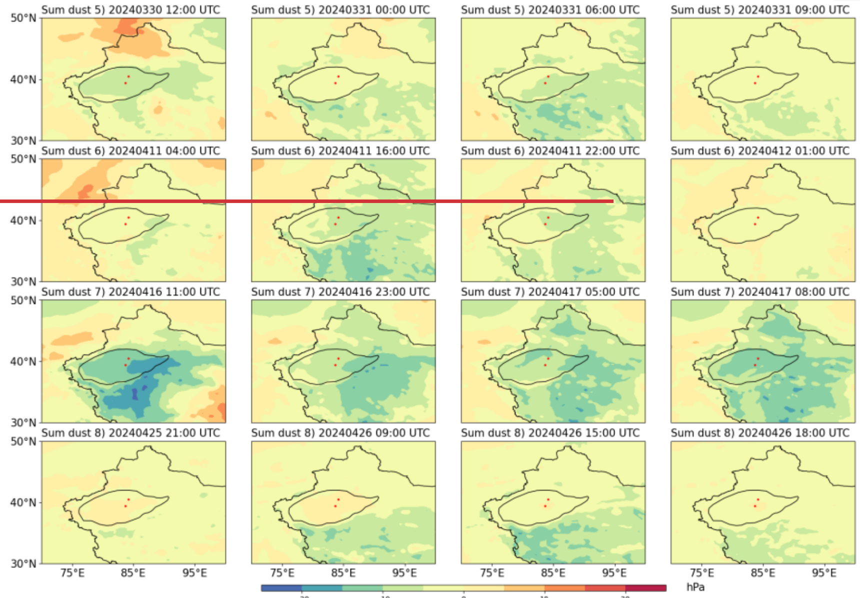

Fig.7 Summer sandstorm ΔP24h,ΔP12h,ΔP6h,ΔP3h pressure difference

Fig.6 and Fig.7 show the changes in average sea-level pressure over the 3, 6, 12, and 24 hours preceding the dust storms in the spring and summer periods, respectively. The calculation method involves subtracting the sea-level pressure at the specified times (3, 6, 12, and 24 hours before the dust storm) from the average sea level pressure at the time of the dust storm. In the figures, higher values indicate a greater increase in pressure, while lower values reflect a larger decrease in pressure.

In ΔP24h, during Dust1-7, the average sea-level pressure in the northern part of the Taklamakan Desert (TD) was lower than at the time of the dust storm. Additionally, for Dust2 and Dust3, the southwestern region also showed a lower pressure than that at the time of the storm. However, in ΔP12h, during Dust1-4, the pressure in the northern and southwestern parts of the Taklamakan Desert (TD) gradually increased but remained lower than the pressure at the time of the dust storm. In contrast, for Dust5-8, the pressure approached that at the time of the storm, and there were no significant changes in the subsequent ΔP6h and ΔP3h periods. For Dust1-4, there was little change in pressure from ΔP6h to ΔP3h, but it still differed significantly from the pressure at the time of the dust storm, especially for Dust3.

In summary, there is a clear difference in the pressure changes before dust storms in the spring and summer in the Taklamakan Desert (TD). In the spring, the pressure changes in the northern or southern parts of TD are significantly larger in ΔP24h compared to the summer, with a gradual increase in pressure in these areas leading up to the storm, forming a noticeable pressure gradient. This is consistent with the pressure difference observed during the dust storm. In the summer, the pressure at TD already approaches that at the time of the storm by ΔP12h, with little change afterward. Therefore, it can be inferred that pressure changes play a more direct and important role in the formation and development of dust storms in spring, while in summer, other factors may have a greater influence on dust storm occurrence.

Tab. 2 Variance and rangeΔP24h,ΔP12h,ΔP6h,ΔP3h before the dust storm

	Variance of ΔP24h	Range of variation	Variance of ΔP12h	Range of variation	Variance of ΔP6h	Range of variation	Variance of ΔP3h	Range of variation
dust1	49.91	(10.66, 24.99)	35.37	(17.82, 9.58)	11.55	(11.37, 10.59)	3.76	(5.75, 8.31)
dust2	34.9	(19.23, 17.15)	28.06	(14.77, 19.90)	16.01	(14.64, 16.75)	7.27	(15.91, 9.53)
dust3	71.14	(17.23, 28.38)	59.21	(25.17, 22.88)	67.81	(25.47, 17.85)	83.14	(24.15, 23.38)
dust4	26.18	(14.89, 14.47)	12.95	(6.59, 15.37)	4.24	(4.99, 9.05)	1.24	(2.84, 6.86)
dust5	19.22	(10.14, 12.81)	10.29	(12.25, 6.52)	11.73	(16.05, 6.41)	3.36	(8.55, 3.61)
dust6	11.47	(8.78, 10.89)	19.8	(16.58, 7.53)	8.25	(11.44, 6.05)	2.66	(6.79, 5.68)

dust7	45.82	(21.66,-14.83)	21.26	(16.02,-6.48)	21.45	(17.80,-6.35)	23.27	(19.91,-5.88)
dust8	2.82	(7.51, 4.75)	10.48	(13.80,-4.47)	11.32	(17.07,-1.61)	3.26	(9.90,-2.63)

Table 2 presents the variance and range of ΔP24h, ΔP12h, ΔP6h, and ΔP3h for the dust storms. Since the pressure difference effectively characterizes pressure changes, its variance reflects the intensity of pressure fluctuations. The analysis reveals that the range and variance in the spring (Dust1-4) are generally larger than in the summer (Dust5-8), indicating that pressure changes before dust storms in the spring are more intense. Notably, the pressure difference between ΔP12h and ΔP6h for Dust1-4 shows significant variation, suggesting that the 12-hour to 6-hour period is when pressure fluctuations are most pronounced. Therefore, ΔP12h and ΔP6h could represent key windows for spring dust storm prediction. Closely monitoring pressure fluctuations during this phase can help predict the occurrence of dust storms in advance.

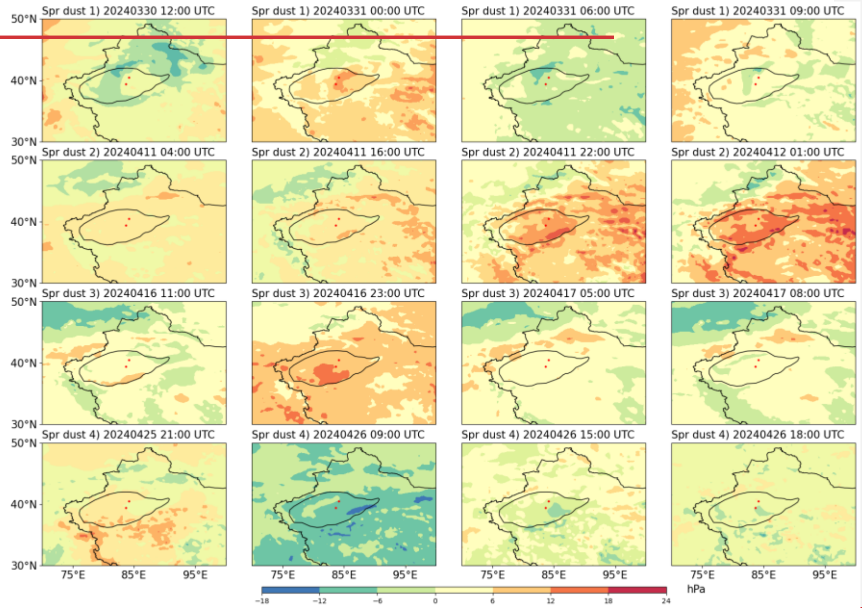

Fig.8 Spring sandstorm Δ 3, Δ 6, Δ 12, Δ 24 temperature difference

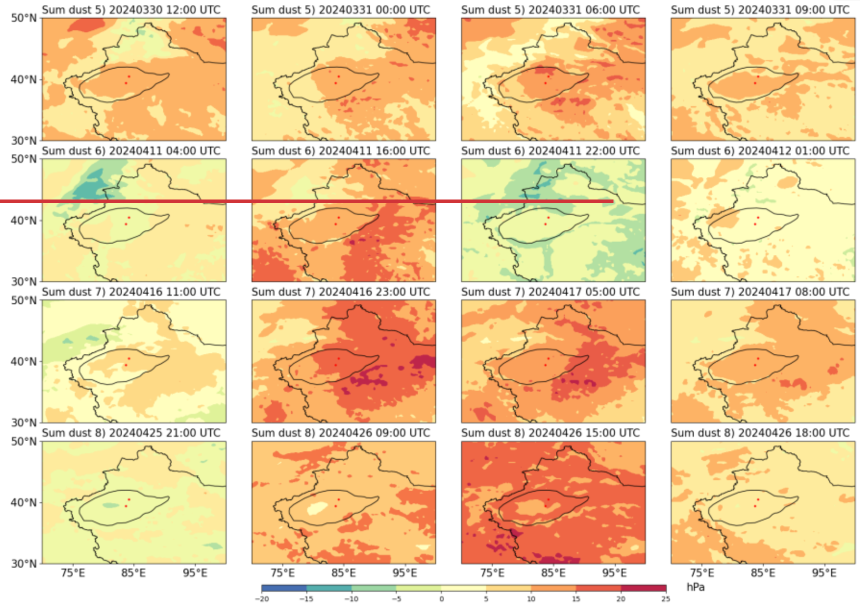

Fig.9 Summer sandstorm Δ 3, Δ 6, Δ 12, Δ 24 temperature difference

In desert regions or inland plateaus, the surface temperature increases dramatically, causing the near-surface air to expand and rise, leading to the formation of upward air currents. Upward air currents can trigger convection in specific areas or create strong winds that stir up surface dust, leading to dust storms. Figures 8 and 9 show the temperature changes 3, 6, 12, and 24 hours before the dust storms in spring and summer. Similar to the calculation of the average sea-level pressure, the larger the value, the lower the current temperature compared to the time of the dust storm, indicating more intense upward movement.

Both in spring and summer, the temperature changes in the Taklamakan Desert (TD) and surrounding areas are influenced by multiple factors, such as time of day and climate conditions, making the temperature variation complex. In spring, there is no clear trend in temperature changes, whereas in summer, most of the time is characterized by warming, particularly in the final three hours. In spring, only Dust2 shows a warming trend, whereas in summer, all processes exhibit a warming trend. Therefore, it can be inferred that temperature changes have a more significant impact on summer dust storms.

Tab. 3 Variance and range 24h, 12h, 6h, and 3h before the dust storm

	Variance of AP24h	Range of variation	Variance of AP12h	Range of variation	Variance of AP6h	Range of variation	Variance of AP3h

dust1	14.75	(-14.72,-11.67)	16.53	(-7.04,-20.38)	8.23	(-11.52,-6.52)	3.7	(-9.70,-2.56)
dust2	10.23	(-11.71,-8.58)	16.8	(-12.25,-14.16)	14.79	(-7.21,-17.02)	11.9	(-7.03,-15.44)
dust3	21.84	(-21.57,-4.40)	18.35	(-12.53,-16.39)	22.47	(-21.32,-8.41)	25.81	(-23.38,-8.48)
dust4	11.57	(-12.32,-11.02)	11.68	(-20.77,-0.23)	5.12	(-14.30,-3.57)	1.44	(-11.28,-5.12)
dust5	12.75	(-14.40,-8.30)	21.95	(-3.87,-22.52)	13.07	(-0.63,-20.23)	1.74	(-2.08,-8.17)
dust6	11	(-13.92,-6.40)	16.46	(-5.59,-20.28)	4.76	(-7.99,-7.40)	1.8	(-7.30,-4.06)
dust7	19.82	(-11.55,-16.01)	29.84	(-10.43,-22.44)	22.69	(-4.06,-27.81)	21.14	(-3.78,-25.95)
dust8	3.71	(-9.98,-6.68)	5.36	(-3.26,-14.72)	5.32	(-2.25,-15.46)	1.99	(-4.24,-8.42)

Table 3 shows the variance and range of temperature differences (ΔT) 24h, 12h, 6h, and 3h before the dust storm. Similar to the variance in pressure differences, the variance rapidly decreases between ΔT12h and ΔT6h, indicating a swift transition from a stable temperature state to an unstable state right before the dust storm occurs. This suggests that the ΔT12h-ΔT6h period is crucial for predicting summer dust storms.

3.4 Tower-observed wind and temperature anomaly profiles~~Dust Flux Analysis~~

带格式的：标题 2，无，缩进：左侧： 0 厘米，悬挂缩进：4.02 字符，段落间距段前：0 磅，段后：0 磅，制表位：不在 3.6 字符

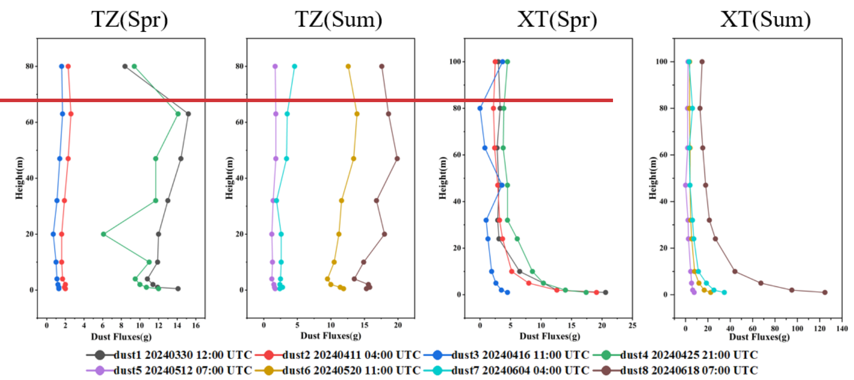

~~Fig.10 Schematic Diagram of Horizontal Dust Flux during Sandstorms (Left: TZ, Right: XT)~~

~~Fig.10 shows the horizontal dust flux (Q) at TZ and XT during spring and summer. The Q at TZ is mainly concentrated between 2g and 10-14g. When Q is low, the dust flux changes smoothly with height, showing no significant fluctuations. However, as Q increases, a noticeable upward trend appears between 47-63 cm, followed by a gradual decline, with a rapid increase in Q below 2m. According to Huo W (2022), the terrain at TZ is more undulating than XT and is influenced by natural dunes. As a result, the dust flux in this area shows an abnormal increase, highlighting the significant impact of topography on dust flux, especially in regions with strong winds or frequent dust activity. In such areas, topography plays a crucial role in dust transport.~~

~~The dust flux (Q) at XT exhibits a pattern similar to that of a parabolic function during spring and summer, gradually increasing as the height decreases. Q remains relatively stable between 100 and 24 meters, with slight fluctuation. However, once the height drops below 24 meters, the Q value rises significantly, especially in the near-surface layer (0 to 2 meters), where dust flux rapidly increases as the height decreases. This is due to the gravitational effect on dust particles, which tend to accumulate near the surface and are more easily lifted by the wind at lower altitudes.~~

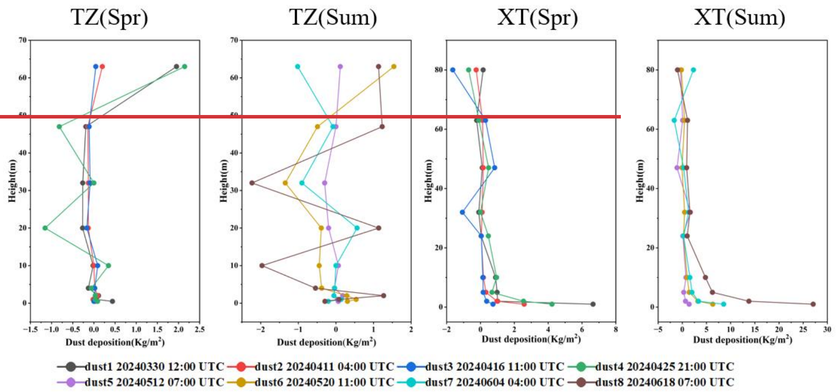

Fig.11 10 Schematic Diagram of Vertical Dust Flux during Sandstorms (Left: TZ, Right: XT)

Fig.11 illustrates the vertical dust flux (F) at TZ and XT during spring and summer. In summer at TZ, the F values fluctuate more significantly. For example, in Dust 8, the F values oscillate between -2 and 1.5 kg/m², showing clear fluctuations. In contrast, the spring F values are more stable, with relatively minor changes; for Dust 1-3, the F values are mainly close to 0, indicating minimal vertical dust movement in the spring at TZ. On the other hand, during the summer, rapid surface temperature rise generates updrafts, causing more pronounced fluctuations in the F values. This suggests that temperature changes strongly influence dust storms at TZ in the summer.

The F curve at XT shows a similar trend to that of Q, exhibiting a pattern resembling a "bell-shaped curve," which suggests that the wind more easily lifts dust as height decreases. Additionally, the F values at XT show a similar trend in spring and summer, without the pronounced influence of temperature rise in TZ. This could be because TZ's more variable topography makes it more susceptible to temperature-induced updrafts. In contrast, XT's relatively flatter terrain may not experience such significant temperature effects, thus leading to more stable vertical dust flux behavior.

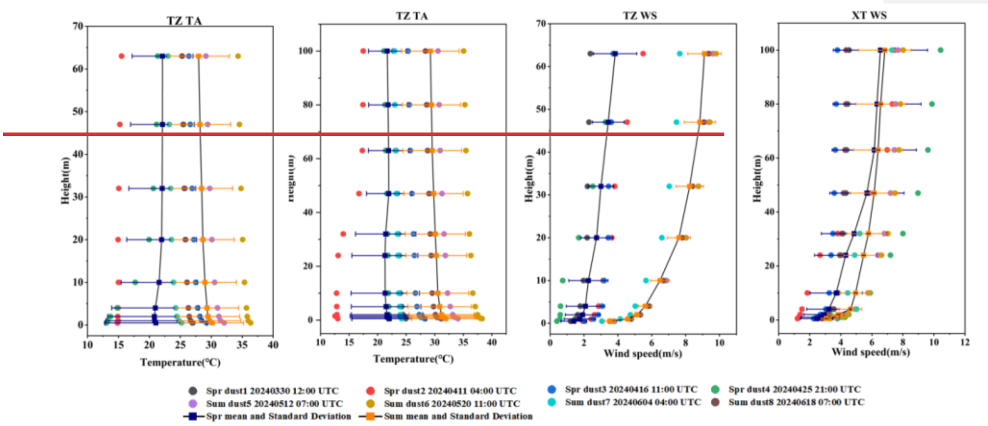

The tower observations further support the regional dynamic and thermal characteristics identified from the ERA5-based analysis. Figure 11 shows the composite evolution of 10 m wind-speed anomaly, 2–10 m wind-shear anomaly, 0.5–10 m air-temperature-difference anomaly, and 2 m air-temperature anomaly from −24 to +3 h relative to dust-storm onset. The 2 m air-temperature anomaly is generally positive before onset, indicating that near-surface warming had already developed during the pre-onset stage. However, this warming signal weakens as onset approaches, whereas the 10 m wind-speed and wind-shear anomalies increase rapidly near onset. This pattern suggests a transition from early thermal preconditioning to enhanced near-surface momentum and wind shear immediately before dust-storm occurrence.

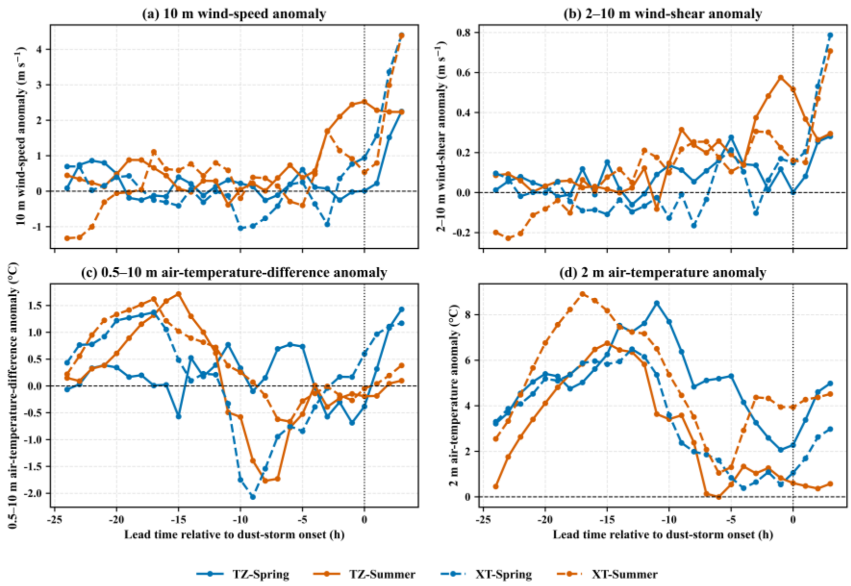

Fig. 11. Composite evolution of tower-observed wind-speed, wind-shear, air-temperature-difference, and 2 m air-temperature anomalies from −24 to +3 h relative to dust-storm onset.

Figure 12 shows the vertical profiles of wind-speed anomalies at TZ and XT. Wind-speed anomalies generally increase before and around dust-storm onset, but their vertical structures differ between the two stations. At XT, especially in summer, positive anomalies become more evident in the lower and middle layers, suggesting stronger near-surface momentum exchange over relatively flat terrain. At TZ, the profiles are more irregular, which may reflect the influence of undulating dune topography and local flow disturbance.

带格式的：缩进：首行缩进： 0 字符

设置了格式：字体：(中文) 宋体，非加粗

带格式的：题目，缩进：首行缩进： 0 厘米

设置了格式：字体：(中文) 宋体

带格式的：两端对齐

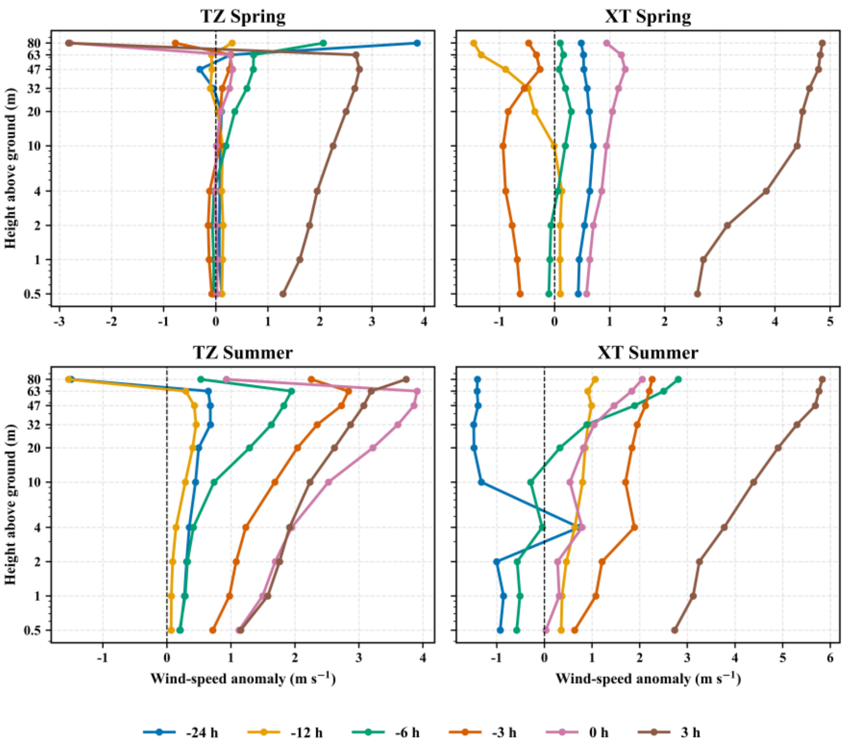

Fig. 12. Vertical profiles of wind-speed anomalies at TZ and XT during spring and summer dust-storm events.

Figure 13 presents the vertical profiles of air-temperature anomalies. In summer, both TZ and XT show stronger positive temperature anomalies than in spring, particularly at XT, where the warming signal is more vertically continuous. This is consistent with the stronger surface heating and boundary-layer development indicated by the ERA5 thermal diagnostics. In spring, the temperature profiles are more irregular, suggesting that thermal forcing was not a common pre-onset signal for all spring events.

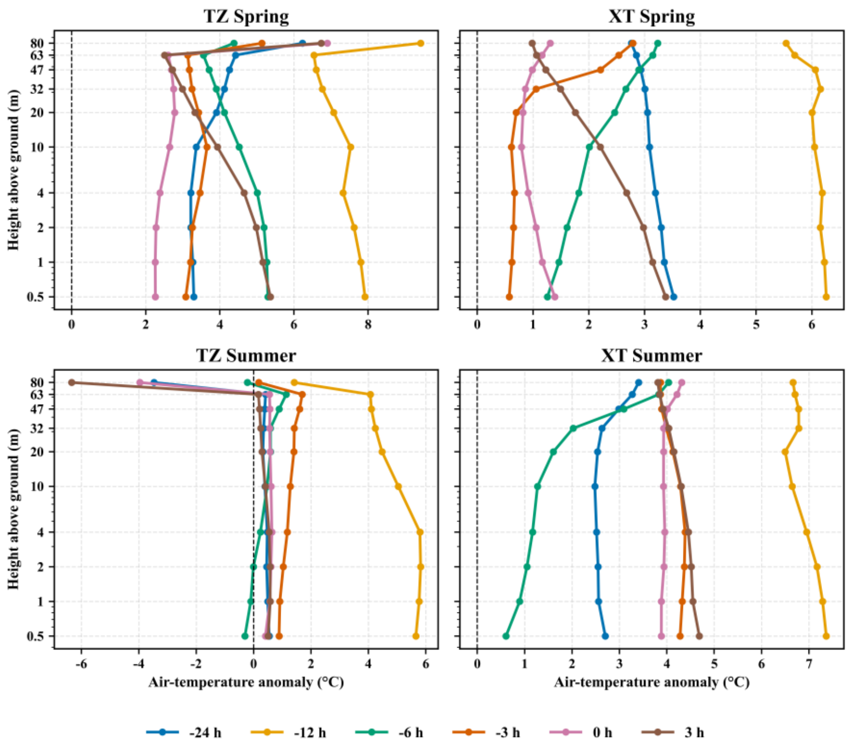

Fig. 13. Vertical profiles of air-temperature anomalies at TZ and XT during spring and summer dust-storm events.

Overall, the tower observations indicate that summer events were more clearly thermally preconditioned in the early stage, while wind-speed and wind-shear enhancement became more evident closer to onset. This station-scale pattern is consistent with the ERA5-based interpretation and shows how regional dynamic and thermal anomalies were expressed in the near-surface layer.

Fig.12 Schematic Diagram of Wind Speed and Temperature during Sandstorms (Left: TZ, Right: XT)

Fig.12 shows the temperature and wind speed variations during sandstorm events at the TZ and XT stations. The figure shows that the average temperature during summer sandstorms is 5-10°C higher than the normal summer temperature. Additionally, during summer sandstorms, the temperature at the lower levels of the stations is significantly higher than at higher levels. In contrast, lower temperatures are lower or comparable to those at higher levels during spring sandstorms.

At both TZ and XT, wind speed decreases with height. Comparing the wind speed variations between spring and summer, the amplitude of the wind speed change in spring is smaller than in summer.

设置了格式：字体：（中文）+中文正文（宋体）
带格式的：题目，缩进：首行缩进： 0 厘米
带格式的：两端对齐

This phenomenon is likely related to the higher surface temperatures in summer, which increase the temperature difference between the surface and the atmosphere, making wind speed changes near the surface more intense. At TZ, the wind speed during summer sandstorms at higher levels is significantly higher than in spring, while the wind speed at lower levels is similar to that of spring. This is likely because spring sandstorms are dominated by horizontal winds, which are influenced by the undulating dunes, resulting in lower wind speeds at higher levels. In contrast, summer sandstorms are dominated by vertical winds and are less influenced by the terrain, thus showing a larger wind speed difference at higher levels. The terrain near the XT station is relatively flat, so the differences in wind speed variations between spring and summer are minor.

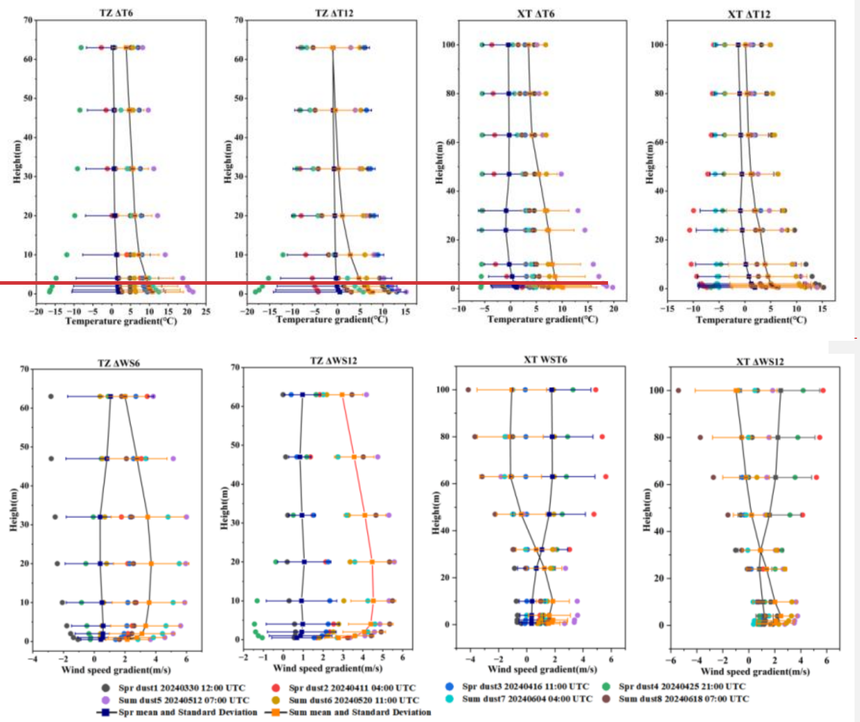

Fig.13 Schematic Diagram of Wind Speed and Temperature Changes (Δ6, Δ12) during Sandstorms (Left: TZ, Right: XT)

Figure 13 shows the temperature and wind speed changes 6 and 12 hours before the sandstorm event. It can be observed that, at both TZ and XT, the average ΔT6 and ΔT12 in summer are higher than those in spring, and the gap between them increases as the height decreases. This indicates that the temperature increase in summer is significantly higher near the surface than in spring, and as the height decreases,

~~the temperature rise becomes more intense.~~

~~The wind speed variation chart for summer at XT shows a decrease in wind speed at higher levels, while wind speed at lower levels increases. In contrast, in spring, wind speed at higher levels increases, and wind speed at lower levels either remains unchanged or slightly increases. This phenomenon may be related to the fact that the XT station is located on the northern edge of TD, where the terrain is flat and not influenced by complex features such as dunes. The reasons for this will be discussed in the discussion section.~~

4 Discussion

The HYSPLIT pathway analysis, ERA5 diagnostics, and tower observations provide complementary evidence for interpreting dust-storm development over the Taklimakan Desert. HYSPLIT identifies the pre-storm airflow pathways reaching the observation sites, ERA5 explains the regional pressure, circulation, and thermal backgrounds behind these pathways, and the tower observations show how these regional conditions are expressed in near-surface wind, temperature, wind shear, and vertical profiles.

The pathway types are closely related to the ERA5 circulation patterns. East-inflow events are generally accompanied by clearer pressure differences between northern Xinjiang, surrounding high-pressure regions, and the Tarim Basin, together with organized 10 m winds entering the desert through the northeastern basin opening. Mountain-crossing events correspond more closely to lower-tropospheric circulation differences around the Tianshan–Pamir region, while the south-to-north pathway is related to pressure and wind configurations along the southern and southwestern margins of the desert. These results indicate that the transport pathways were not isolated trajectory features, but were linked to regional dynamic backgrounds and basin topographic constraints.

ERA5 further reveals a seasonal shift in the pre-onset conditions. Spring events show stronger and more persistent mean sea-level pressure-gradient and 850 hPa height-gradient anomalies, consistent with the more distinct dynamic pathways. Summer events show weaker pressure-gradient organization but stronger early thermal anomalies, including enhanced net shortwave radiation, surface–air temperature difference, and boundary-layer height. This suggests that spring dust storms were more closely related to regional dynamic forcing, whereas summer events were more strongly influenced by early thermal preconditioning.

The tower observations provide station-scale support for this interpretation. Summer events show more continuous vertical warming, while wind-speed and wind-shear anomalies strengthen closer to onset, indicating that thermal preconditioning alone is insufficient and that near-surface momentum enhancement remains necessary. The differences between TZ and XT further suggest that local terrain can modify the near-surface response to regional forcing. XT shows more regular vertical structures, whereas TZ exhibits more variable profiles, likely related to dune-induced flow disturbance and heterogeneous roughness.

Several uncertainties remain. The analysis is based on eight events from one field season, and the identified pathway and seasonal characteristics need to be tested using longer-term samples. In addition, the lack of direct turbulence, vertical velocity, and lidar observations limits the interpretation of vertical transport processes. Future studies should combine multi-year observations, turbulence measurements, lidar data, and high-resolution simulations to better distinguish the roles of synoptic forcing, thermal instability, and local terrain heterogeneity.

5 Conclusion

带格式的：标题 1，缩进：首行缩进： 0 厘米

This study examined eight complete dust-storm events over the Taklimakan Desert using HYSPLIT trajectories, ERA5 reanalysis, and dual-gradient tower observations. The main conclusions are as follows.

The analyzed events exhibited three main types of pre-storm airflow transport pathways: east-inflow transport through the northeastern opening of the Tarim Basin, mountain-crossing transport across the Tianshan–Pamir region, and south-to-north transport related to airflows crossing the Tibetan Plateau and Kunlun Mountains.

ERA5 analysis shows that these pathways were closely linked to regional dynamic and thermal backgrounds. Spring events were associated with stronger pressure-gradient and 850 hPa height-gradient anomalies, corresponding to more distinct dynamically driven pathways. Summer events showed weaker pressure-gradient signals but stronger early thermal anomalies, indicating more evident thermal preconditioning before onset.

The tower observations were consistent with the ERA5-based interpretation. Summer events showed stronger positive temperature anomalies and more continuous vertical warming, while wind-speed and wind-shear anomalies strengthened closer to onset. This indicates a staged process from early background adjustment to near-surface wind enhancement.

The two stations showed different vertical responses. XT displayed more regular wind and temperature anomaly structures, whereas TZ showed more variable profiles, suggesting that local terrain heterogeneity may modulate the near-surface response to regional dynamic and thermal forcing.

Overall, Taklimakan dust-storm development is shaped by the interaction among regional airflow pathways, dynamic–thermal background conditions, near-surface wind response, and local terrain effects.

4 Discussion

4.1 Dust Trajectory Analysis

带格式的: 左, 1 级, 右侧: 1.11 厘米, 段落间距段前: 1.5 行, 段后: 1 行, 孤行控制, 制表位: 不在 3.6 字符

This study analyzes eight dust storm events in TD from March to June. Through trajectory analysis, it was found that the paths of dust storms entering the desert interior exhibit significant diversity, but can be summarized into three main types.

The first type is the "East-Inflow" path, where most dust storms move from northeast to southwest. This path's formation is likely closely related to the topography surrounding TD: the northern and western parts of the desert are surrounded by high mountain ranges, while the eastern area has lower terrain, including the low-lying Lop Nur region. When a strong high-pressure system occurs in the northern regions, strong winds enter the desert through the lower terrain gaps, thus forming the East-Inflow path. The second type is the "Mountain-Crossing" path, where some strong winds enter the desert by crossing the western Tianshan Mountains or the Pamir Plateau. However, winds along this path are typically concentrated in the upper atmospheric layers, and their intensity is limited. The topographical barrier effect weakens the surface wind speed, with more of the driving force concentrated in the middle and upper levels of the atmosphere. The third type is the "Westward" path, primarily occurring during the two dust storms after June, with the trajectories moving from west to east. This path is likely related to the climatic characteristics of Central Asia. As summer arrives, the surface heating in the inland areas of Central Asia becomes more pronounced, leading to higher surface air temperatures around the desert. This temperature contrast affects the direction of air flow. When the dust storm approaches the desert, the larger surface-to-atmosphere temperature difference may cause a change in the direction of the airflow.

4.2 Discussion of Dynamic and Thermal Factors

This study further reveals the impact of dynamic and thermal mechanisms on dust storm processes. Analysis of the ERA5 data shows that from March to April, the TD region and its surroundings exhibit stronger pressure gradients, which favor the formation of strong winds. Additionally, within 24 hours before the dust storm event, spring sees significantly more dramatic pressure changes, aligning with the dynamic-dominated mechanism during this period. From May to June, the temperature at the desert surface rises significantly, increasing the temperature difference between the surface and the atmosphere. Furthermore, 24 hours before the dust storm, surface temperatures tend to increase in summer; in spring, temperatures either decrease or remain constant. This indicates that thermal factors dominate the formation of dust storms during the summer months.

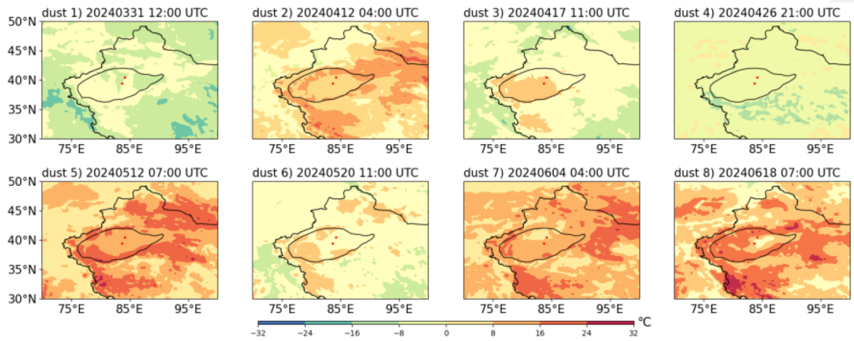

Fig.14 Temperature Difference in Dust Storms (Dust1-8)

To better explore the impact of temperature on dust storms, Figure 14 shows the surface-atmosphere temperature difference for Dust1-8. It can be observed that, except for Dust6, which occurred in the afternoon, the surface-atmosphere temperature difference in summer around TD and its surrounding areas is significantly higher than in spring. Additionally, from the periphery to the interior of TD, the temperature difference gradually decreases, indicating a transition from an unstable to a stable atmosphere, which suggests that dust is moving from the periphery of TD toward the desert interior.

Analysis of observational data reveals that in summer, both TZ and XT experience higher temperatures than in spring, with the temperature rise before dust storms being significantly greater in summer. Moreover, as height decreases, the temperature change becomes more intense. In contrast, the temperature difference in spring remains roughly around 0°C with height changes. This suggests that in the TD region, the overall temperature is higher in summer. However, the temperature increase is also significantly larger than in spring, especially in the lower altitude areas. Therefore, it can be inferred that spring temperature has a relatively minor impact on dust storms, while temperature in summer has a significantly larger effect.

For XT, the wind speed difference between spring and summer shows two distinctly different patterns. In summer, the wind speed at higher levels decreases, while at lower levels, it increases. In spring, the wind speed at higher levels increases, while the wind speed at lower levels remains constant or slightly increases. This could be due to the higher surface temperatures in summer, which increase the temperature difference and lead to intense convection, promoting updrafts and intensifying low-level wind speeds. At higher levels, the wind speed slightly decreases due to air sinking and a more stable atmosphere. In spring, with lower surface temperatures and smaller temperature differences, convection is weakened, and high-level wind speeds increase due to enhanced vertical stability. In contrast, low-level wind speeds remain relatively unchanged.

A comprehensive analysis from point to area was conducted by combining reanalysis data and observational data, further proving the seasonal differences in dust storm formation in the TD region. In spring, the primary driving force of dust storms is the pressure gradient, where the significant horizontal pressure difference leads to strong wind processes, triggering dust storms. In contrast, dust storms are mainly influenced by the difference in surface-atmosphere temperature in summer. The significant temperature contrast between the surface and the atmosphere creates intense instability, promoting enhanced convective activity and thereby intensifying the occurrence of dust storms. This multi-angle verification, from localized observations to regional reanalysis, further clarifies the dominant roles of dynamic and thermal factors in different seasons.

4.3 Key parameters are influenced by the terrain.

At the XT station (representing flat terrain), the dust flux (Q) exhibits a clear power-law function characteristic. In contrast, at the TZ station (representing undulating terrain), the dust flux (Q) shows a phased variation pattern. When Q values are high, an initial upward trend is followed by a decline, and then another increase. This variation may be attributed to secondary dust sources from the surrounding dunes, particularly influencing the mid-layer observational data, which causes an increase in dust flux within a specific altitude range. F exhibits a pattern similar to that of Q, but with more significant terrain differences. At the XT station, F remains relatively stable, whereas at the TZ station, F stabilizes around 0 kg/m^2 in spring. However, the variation increases in summer, oscillating between -2 and 1.5 kg/m^2. This phenomenon is likely due to the dominant influence of summer temperatures on vertical air currents.

5 Conclusion

The study is based on a dual gradient observational experiment conducted in the central and peripheral regions of the Taklamakan Desert (TD), with eight observational samples obtained from April to June. Combined with ERA5 reanalysis data and the HYSPLIT backward trajectory model, the following conclusions were drawn:

The dust storm trajectories in the Taklamakan Desert (TD) can be classified into three types: first, dust storms travel from east to west, passing through the gaps in the Tianshan Mountains; second, they traverse the western Tianshan and the Pamir Plateau; and finally, after the onset of summer in June, the dust storm trajectories are dominated by thermal factors, initially moving from west to east, and then shifting from the northeast to the southwest into the desert.

Dynamic factors primarily drive dust storms in the TD in March and April, where strong winds caused by pressure gradients lead to dust storms. In May and June, thermal factors dominate, with temperature differences between the surface and the atmosphere triggering convection that results in dust storms. Additionally, the period 12 to 6 hours before the dust storm is characterized by significant changes in atmospheric pressure and temperature, which can be used as a key time window for predicting the occurrence of dust storms.

At the XT station, representing flat terrain, Q and F rapidly increase near the surface, following a power-law function pattern. At the TZ station, representing undulating terrain, Q shows a similar power-law function like curve when values are high. However, fluctuations in mid-level Q are caused by secondary dust sources from dunes. On the other hand, F is influenced by both terrain and thermal factors, with minor fluctuations in spring and larger fluctuations in summer. During summer, both stations experience significantly higher temperatures and more pronounced temperature changes compared to spring, highlighting the more decisive influence of summer temperatures on dust storms. Additionally, the variability in wind speed at the XT station during summer indicates that wind speed changes are primarily influenced by seasonal temperature differences, convective intensity, and the flat terrain of the area.

Acknowledgements

We gratefully acknowledge the National Earth System Science Data Center (http://www.geodata.cn) and the Institute of Desert Meteorology (China Meteorological Administration, Urumqi) for providing essential datasets. We also extend our thanks to the College of Geography and Remote Sensing Science, Xinjiang University (Urumqi), for their technical support.

Author Contributions

Y.W. : Conceptualization , Writing – original draft , Formal Analysis.
WH.:Methodology, Supervision, Writing - review. & editing.
YL.:Validation.
M.M : Investigation, Data Curation.
F.Y: Experimental Design, Supervision.
C.Z..X.Y.A.M.: Investigation , Data Curation.

Funding

This work was supported by the Tianshan Talent Project of Xinjiang (Grant No. 2023TSYCCX0075), the China Meteorological Administration Youth Innovation Team Project (Grant No. CMA2024QN13), the National Natural Science Foundation of China (42207134), and the Xinjiang Science and Technology Innovation Team (Tianshan Innovation Team) Project (Grant No. 2022TSYCTD0007).

Data availability

The meteorological observational data used in this study are maintained and owned by the Institute of Desert Meteorology, China Meteorological Administration, located in Urumqi, Xinjiang, China, and are subject to institutional regulations and access restrictions. ERA5 reanalysis datasets were obtained from the European Centre for Medium-Range Weather Forecasts (ECMWF) through the Copernicus Climate Data Store (https://cds.climate.copernicus.eu). Researchers or interested parties who wish to obtain access to the observational datasets may submit a formal request to the

Institute of Desert Meteorology, outlining the purpose and scope of their intended use. Approval of such requests will be at the discretion of the institute, in accordance with its data-sharing policies.

Competing Interests

The authors declare no competing interests.

References

Achakulwisut, P., Mickley, L. J., and Anenberg, S. C.: Drought-sensitivity of fine dust in the US Southwest: Implications for air quality and public health under future climate change, Environ. Res. Lett., 13, 054025, https://doi.org/10.1088/1748-9326/aabf20, 2018.

Aili, A., Xu, H., Kasim, T., and Abulikemu, A.: Origin and Transport Pathway of Dust Storm and Its Contribution to Particulate Air Pollution in Northeast Edge of Taklimakan Desert, China, Atmosphere, 12, 113, https://doi.org/10.3390/atmos12010113, 2021.

Aili, A., Xu, H., Xu, Q., and Liu, K.: Aeolian dust movement and deposition under local atmospheric circulation in a desert-oasis transition zone of the northeastern Taklimakan desert, Ecological Indicators, 157, 111289, https://doi.org/10.1016/j.ecolind.2023.111289, 2023.

Aili, A., Waheed, A., Zhao, X., and Xu, H.: Establishing an Early Warning System for Dust Storms in Peri-Desert Regions, Environments, 11, 61, https://doi.org/10.3390/environments11040061, 2024.

Bao, C. and Fang, C.: Water resources constraint force on urbanization in water deficient regions: A case study of the Hexi Corridor, arid area of NW China, Ecological Economics, 62, 508–517, https://doi.org/10.1016/j.ecolecon.2006.07.013, 2007.

带格式的：书目，定义网格后自动调整右缩进，调整中文与西文文字的间距，调整中文与数字的间距

域代码已更改

Bao, T., Xi, G., Hao, Y., Chang, I.-S., Wu, J., Xue, Z., Jin, E., Zhang, W., and Bao, Y.: The Transport Path and Vertical Structure of Dust Storms in East Asia and the Impacts on Cities in Northern China, Remote Sensing, https://doi.org/10.3390/rs15123183, 2023.

Bi, J., Li, Z., Zuo, D., Yang, F., Li, B., Ma, J., Huang, Z., and He, Q.: Dust Aerosol Vertical Profiles in the Hinterland of Taklimakan Desert During Summer 2019, Front. Environ. Sci., 10, 851915, https://doi.org/10.3389/fenvs.2022.851915, 2022.

Chen, S., Zhao, D., Huang, J., He, J., Chen, Y., Chen, J., Bi, H., Lou, G., Du, S., Zhang, Y., and Yang, F.: Mongolia Contributed More than 42% of the Dust Concentrations in Northern China in March and April 2023, Adv. Atmos. Sci., 40, 1549–1557, https://doi.org/10.1007/s00376-023-3062-1, 2023a.

Chen, Y., An, J., Qu, Y., Xie, F., and Ma, S.: Dust radiation effect on the weather and dust transport over the Taklimakan Desert, China, Atmospheric Research, 284, 106600, https://doi.org/10.1016/j.atmosres.2022.106600, 2023b.

Gao, X., Wang, D., Gui, H., and et al: Dominant circulation pattern and moving path of the Mongolian Cyclone for the severe sand and dust storm in China, Atmospheric Research, https://doi.org/10.1016/j.atmosres.2024.107272, 2024.

Ge, J. M., Huang, J. P., Xu, C. P., Qi, Y. L., and Liu, H. Y.: Characteristics of Taklimakan dust emission and distribution: A satellite and reanalysis field perspective: Taklimakan dust Characteristics, J. Geophys. Res. Atmos., 119, 11,772-11,783, https://doi.org/10.1002/2014JD022280, 2014.

Gillette, D. A. and Passi, R.: Modeling dust emission caused by wind erosion, J. Geophys. Res., 93, 14233–14242, https://doi.org/10.1029/JD093iD11p14233, 1988.

Huo, W., Song, M., Wu, Y., Zhi, X., Yang, F., Ma, M., Zhou, C., Yang, X., Mamtimin, A., and He, Q.: Relationships between Near-Surface Horizontal Dust Fluxes and Dust Depositions at the Centre and Edge of the Taklamakan Desert, Land, 11, 959, https://doi.org/10.3390/land11070959, 2022.

Iversen, J. D. and White, B. R.: Saltation threshold on Earth, Mars and Venus, Sedimentology, 29, 111–119, https://doi.org/10.1111/j.1365-3091.1982.tb01713.x, 1982.

Kai, Z. and Huiwang, G.: The characteristics of Asian-dust storms during 2000–2002: From the source to the sea, Atmospheric Environment, 41, 9136–9145, https://doi.org/10.1016/j.atmosenv.2007.08.007, 2007.

Kok, J. F., Storelvmo, T., Karydis, V. A., Adebiyi, A. A., Mahowald, N. M., Evan, A. T., He, C., and Leung, D. M.: Mineral Dust Aerosol Impacts on Global Climate and Climate Change, Nat. Rev. Earth Environ., 4, 71–86, https://doi.org/10.1038/s43017-022-00379-5, 2023.

Li, J., Han, Y., Liu, W., Cao, L., and Lu, Z.: Contributions of gust under stationery weather conditions to the dust aerosol budget in northwestern China, Atmospheric Research, 293, 106914, https://doi.org/10.1016/j.atmosres.2023.106914, 2023.

Liu, X., Yin, Z., Zhang, X., and Yang, X.: Analyses of the spring dust storm frequency of northern China in relation to antecedent and concurrent wind, precipitation, vegetation, and soil moisture conditions, J. Geophys. Res., 109, 2004JD004615, https://doi.org/10.1029/2004JD004615, 2004.

Manisalidis, I., Stavropoulou, E., Stavropoulos, A., and Bezirtzoglou, E.: Environmental and Health Impacts of Air Pollution: A Review, Front. Public Health, 8, 14, https://doi.org/10.3389/fpubh.2020.00014, 2020.

Marticorena, B. and Bergametti, G.: Modeling the atmospheric dust cycle: 1. Design of a soil-derived dust emission scheme, J. Geophys. Res., 100, 16415–16430, https://doi.org/10.1029/95JD00690, 1995.

Mu, F. and Fiedler, S.: How much do atmospheric depressions and Mongolian cyclones contribute to spring dust activities in East Asia?, npj Clim Atmos Sci, 8, 51, https://doi.org/10.1038/s41612-025-00929-w, 2025.

Prospero, J. M.: Long-range transport of mineral dust in the global atmosphere: Impact of African dust on the environment of the southeastern United States, Proc. Natl. Acad. Sci. U.S.A., 96, 3396–3403, https://doi.org/10.1073/pnas.96.7.3396, 1999.

Raupach, M. R.: Drag and drag partition on rough surfaces, Boundary-Layer Meteorol, 60, 375–395, https://doi.org/10.1007/BF00155203, 1992.

Shao, Y. and Dong, C. H.: A review on East Asian dust storm climate, modelling and monitoring, Global and Planetary Change, 52, 1–22, https://doi.org/10.1016/j.gloplacha.2006.02.011, 2006.

Stein, A. F., Draxler, R. R., Rolph, G. D., Stunder, B. J. B., Cohen, M. D., and Ngan, F.: NOAA's HYSPLIT Atmospheric Transport and Dispersion Modeling System, Bulletin of the American Meteorological Society, 96, 2059–2077, https://doi.org/10.1175/BAMS-D-14-00110.1, 2015.

Su, L., Lu, C., Yuan, J., Wang, X., He, Q., and Xia, H.: Measurement report: The promotion of low-level jet and thermal-effect on development of deep convective boundary layer at the southern edge of the Taklimakan Desert, https://doi.org/10.5194/egusphere-2024-1010, 15 May 2024.

Sun, J. and Liu, T.: The Age of the Taklimakan Desert, Science, 312, 1621–1621, https://doi.org/10.1126/science.1124616, 2006.

Tong, D., Feng, I., Gill, T. E., Schepanski, K., and Wang, J.: How Many People Were Killed by Windblown Dust Events in the United States?, Bulletin of the American Meteorological Society, 104, E1067–E1084, https://doi.org/10.1175/BAMS-D-22-0186.1, 2023.

Wang, B., Ji, H., Zhang, Z., Liang, J., Zhang, L., Li, M., Qiu, R., Luo, H., An, W., Tian, P., and Amonov, M. O.: Surface-Dependent Meteorological Responses to a Taklimakan Dust Event During Summer near the Northern Slope of the Tibetan Plateau, Remote Sensing, 17, 1561, https://doi.org/10.3390/rs17091561, 2025.

Wang, H., Jia, X., Li, K., and Li, Y.: Horizontal wind erosion flux and potential dust emission in arid and semiarid regions of China: A major source area for East Asia dust storms, CATENA, 133, 373–384, https://doi.org/10.1016/j.catena.2015.06.011, 2015.

Wang, X., Zhai, P., and Wang, C.: Variations in extratropical cyclone activity in northern East Asia, Adv. Atmos. Sci., 26, 471–479, https://doi.org/10.1007/s00376-009-0471-8, 2009.

Wang, Y., Gao, J., Mamtimin, A., Sayit, H., Zhou, C., Li, R., Dawut, M., Yang, F., Huo, W., Wen, C., Song, M., and Aihaiti, A.: Evolution law of atmospheric boundary layer in Gurbantünggüt Desert based on reanalysis dataset and in situ observation data, Heliyon, 9, e14147, https://doi.org/10.1016/j.heliyon.2023.e14147, 2023.

Wen, H.-J., Wang, S.-L., Wu, C.-D., and Liang, M.-C.: Association of Asian dust storms and PM2.5 with clinical visits for respiratory diseases in children, Atmospheric Environment, 333, 120631, https://doi.org/10.1016/j.atmosenv.2024.120631, 2024.

Xing, Y., Chen, Y., Yan, S., Cao, X., Zhou, Y., Zhang, X., Shi, T., Niu, X., Wu, D., Cui, J., Zhou, Y., Wang, X., and Pu, W.: Dust storms from the Taklamakan Desert significantly darken snow surface on surrounding mountains, Atmos. Chem. Phys., 24, 5199–5219, https://doi.org/10.5194/acp-24-5199-2024, 2024.

Xiong, Z., Xu, X., Yang, Y., and Luo, T.: Diurnal vertical distribution and transport of dust aerosol over and around Tibetan Plateau from lidar on International Space Station, Atmospheric Research, 294, 106939, https://doi.org/10.1016/j.atmosres.2023.106939, 2023.

Xu, C., Guan, Q., Lin, J., Luo, H., Yang, L., Tan, Z., Wang, Q., Wang, N., and Tian, J.: Spatiotemporal variations and driving factors of dust storm events in northern China based on high-temporal-resolution analysis of meteorological data (1960–2007), Environmental Pollution, 260, 114084, https://doi.org/10.1016/j.envpol.2020.114084, 2020.

Yang, X., Shen, S., Yang, F., He, Q., Ali, M., Huo, W., and Liu, X.: Spatial and temporal variations of blowing dust events in the Taklimakan Desert, Theor Appl Climatol, 125, 669–677, https://doi.org/10.1007/s00704-015-1537-4, 2016.

Yuan, T., Chen, S., Huang, J., Wu, D., Lu, H., Zhang, G., Ma, X., Chen, Z., Luo, Y., and Ma, X.: Influence of Dynamic and Thermal Forcing on the Meridional Transport of Taklimakan Desert Dust in Spring and Summer, J. Climate, 32, 749–767, https://doi.org/10.1175/JCLI-D-18-0361.1, 2019.

Zeng, X. and Dickinson, R. E.: Effect of Surface Sublayer on Surface Skin Temperature and Fluxes, J. Climate, 11, 537–550, https://doi.org/10.1175/1520-0442(1998)011%3C0537:EOSSOS%3E2.0.CO;2, 1998.

Zhang, H., Cisse, M., Dauphin, Y. N., and Lopez-Paz, D.: mixup: Beyond Empirical Risk Minimization, https://doi.org/10.48550/ARXIV.1710.09412, 2017.

Zhang, L., Zhang, H., Cai, X., Song, Y., Mamtimin, A., and He, Q.: Physical Mechanisms of Deep Convective Boundary Layer Leading to Dust Emission in the Taklimakan Desert, GEOPHYSICAL RESEARCH LETTERS, 51, e2024GL108521, https://doi.org/10.1029/2024gl108521, 2024.

Zhang, X., Wang, T., Wang, S., Jiao, Y., Tang, J., Li, J., Yang, F., Amonov, M. O., and Abdullaev, S. F.: Conducive circulation patterns and transport mechanisms for spring dust from Taklimakan Desert to the Tibetan Plateau, Environment International, 197, 109356, https://doi.org/10.1016/j.envint.2025.109356, 2025.

~~Achakulwisut, P., Mickley, L. J., & Anenberg, S. C. (2018). Drought-sensitivity of~~

fine dust in the US Southwest: Implications for air quality and public health under future climate change. *Environmental Research Letters*, *13*(5), 054025. https://doi.org/10.1088/1748-9326/aabf20

Aili, A., Xu, H., Xu, Q., & Liu, K. (2023). Aeolian dust movement and deposition under local atmospheric circulation in a desert-oasis transition zone of the northeastern Taklimakan desert. *Ecological Indicators*, *157*, 111289. https://doi.org/10.1016/j.ecolind.2023.111289

Bao, C., & Fang, C. (2007). Water resources constraint force on urbanization in water deficient regions: A case study of the Hexi Corridor, arid area of NW China. *Ecological Economics*, *62*(3–4), 508–517. https://doi.org/10.1016/j.ecolecon.2006.07.013

Chen, S., Zhao, D., Huang, J., He, J., Chen, Y., Chen, J., Bi, H., Lou, G., Du, S., Zhang, Y., & Yang, F. (2023a). Mongolia Contributed More than 42% of the Dust Concentrations in Northern China in March and April 2023. *Advances in Atmospheric Sciences*, *40*(9), 1549–1557. https://doi.org/10.1007/s00376-023-3062-1

Chen, S., Zhao, D., Huang, J., He, J., Chen, Y., Chen, J., Bi, H., Lou, G., Du, S., Zhang, Y., & Yang, F. (2023b). Mongolia Contributed More than 42% of the Dust Concentrations in Northern China in March and April 2023. *Advances in Atmospheric Sciences*, *40*(9), 1549–1557. https://doi.org/10.1007/s00376-023-3062-1

Chen, Y., An, J., Qu, Y., Xie, F., & Ma, S. (2023). Dust radiation effect on the weather and dust transport over the Taklimakan Desert, China. *Atmospheric Research*, *284*, 106600. https://doi.org/10.1016/j.atmosres.2022.106600

DeMeester, T. R., & Johnson, L. F. (1975). Evaluation of the Nissen antireflux procedure by esophageal manometry and twenty-four hour pH monitoring. *American Journal of Surgery*, *129*(1), 94–100. https://doi.org/10.1016/0002-9610(75)90174-9

Gillette, D. A., & Passi, R. (1988). Modeling dust emission caused by wind erosion. *Journal of Geophysical Research: Atmospheres*, *93*(D11), 14233–14242. https://doi.org/10.1029/JD093iD11p14233

Hosseini Dehshiri, S. S., & Firoozabadi, B. (2024). Dust emission, transport, and deposition in central Iran and their radiative forcing effects: A numerical simulation.

Atmospheric Pollution Research, *15*(11), 102267. https://doi.org/10.1016/j.apr.2024.102267

Huo, W., Song, M., Wu, Y., Zhi, X., Yang, F., Ma, M., Zhou, C., Yang, X., Mamtimin, A., & He, Q. (2022). Relationships between Near-Surface Horizontal Dust Fluxes and Dust Depositions at the Centre and Edge of the Taklamakan Desert. *Land*, *11*(7), 959. https://doi.org/10.3390/land11070959

Iversen, J. D., & White, B. R. (1982). Saltation threshold on Earth, Mars and Venus. *Sedimentology*, *29*(1), 111–119. https://doi.org/10.1111/j.1365-3091.1982.tb01713.x

Kai, Z., & Huiwang, G. (2007). The characteristics of Asian-dust storms during 2000–2002: From the source to the sea. *Atmospheric Environment*, *41*(39), 9136–9145. https://doi.org/10.1016/j.atmosenv.2007.08.007

Liu, J. T., Jiang, X. G., Zheng, X. J., Kang, L., & Qi, F. Y. (2004). An Intensive Mongolian Cyclone Genesis Induced Severe Dust Storm. *Terrestrial, Atmospheric and Oceanic Sciences*, *15*(5), 1019. https://doi.org/10.3319/TAO.2004.15.5.1019(ADSE)

Ma, M., Yang, X., He, Q., Zhou, C., Mamtimin, A., Huo, W., & Yang, F. (2020). Characteristics of dust devil and its dust emission in northern margin of the Taklimakan Desert. *Aeolian Research*, *44*, 100579. https://doi.org/10.1016/j.aeolia.2020.100579

MacKinnon, D. J., Clow, G. D., Tigges, R. K., Reynolds, R. L., & Chavez, P. S. (2004). Comparison of aerodynamically and model-derived roughness lengths (zo) over diverse surfaces, central Mojave Desert, California, USA. *Geomorphology*, *63*(1–2), 103–113. https://doi.org/10.1016/j.geomorph.2004.03.009

Manisalidis, I., Stavropoulou, E., Stavropoulos, A., & Bezirtzoglou, E. (2020). Environmental and Health Impacts of Air Pollution: A Review. *Frontiers in Public Health*, *8*, 14. https://doi.org/10.3389/fpubh.2020.00014

Marticorena, B., & Bergametti, G. (1995). Modeling the atmospheric dust cycle: 1. Design of a soil-derived dust emission scheme. *Journal of Geophysical Research: Atmospheres*, *100*(D8), 16415–16430. https://doi.org/10.1029/95JD00690

Mohebbi, A., Green, G. T., Akbariyeh, S., Yu, F., Russo, B. J., & Smaglik, E. J. (2019). Development of Dust Storm Modeling for Use in Freeway Safety and Operations Management: An Arizona Case Study. *Transportation Research Record:*

Journal of the Transportation Research Board, *2673*(5), 175–187. https://doi.org/10.1177/0361198119839978

Perez, L., Tobias, A., Querol, X., Künzli, N., Pey, J., Alastuey, A., Viana, M., Valero, N., González-Cabré, M., & Sunyer, J. (2008). Coarse Particles From Saharan Dust and Daily Mortality. *Epidemiology*, *19*(6), 800–807. https://doi.org/10.1097/EDE.0b013e31818131cf

Prospero, J. M. (1999). Long-range transport of mineral dust in the global atmosphere: Impact of African dust on the environment of the southeastern United States. *Proceedings of the National Academy of Sciences*, *96*(7), 3396–3403. https://doi.org/10.1073/pnas.96.7.3396

Raupach, M. R. (1992). Drag and drag partition on rough surfaces. *Boundary-Layer Meteorology*, *60*(4), 375–395. https://doi.org/10.1007/BF00155203

Rizza, U., Barnaba, F., Miglietta, M. M., Mangia, C., Di Liberto, L., Dionisi, D., Costabile, F., Grasso, F., & Gobbi, G. P. (2017). WRF-Chem model simulations of a dust outbreak over the central Mediterranean and comparison with multi-sensor desert dust observations. *Atmospheric Chemistry and Physics*, *17*(1), 93–115. https://doi.org/10.5194/acp-17-93-2017

Shao, Y., & Dong, C. H. (2006). A review on East Asian dust storm climate, modelling and monitoring. *Global and Planetary Change*, *52*(1–4), 1–22. https://doi.org/10.1016/j.gloplacha.2006.02.011

Stein, A. F., Draxler, R. R., Rolph, G. D., Stunder, B. J. B., Cohen, M. D., & Ngan, F. (2015). NOAA's HYSPLIT Atmospheric Transport and Dispersion Modeling System. *Bulletin of the American Meteorological Society*, *96*(12), 2059–2077. https://doi.org/10.1175/BAMS-D-14-00110.1

Sun, J., & Liu, T. (2006). The Age of the Taklimakan Desert. *Science*, *312*(5780), 1621–1621. https://doi.org/10.1126/science.1124616

Tong, D., Feng, I., Gill, T. E., Schepanski, K., & Wang, J. (2023). How Many People Were Killed by Windblown Dust Events in the United States? *Bulletin of the American Meteorological Society*, *104*(5), E1067–E1084. https://doi.org/10.1175/BAMS-D-22-0186.1

Wang, H., Jia, X., Li, K., & Li, Y. (2015). Horizontal wind erosion flux and potential dust emission in arid and semiarid regions of China: A major source area for East Asia dust storms. *CATENA*, *133*, 373–384. https://doi.org/10.1016/j.catena.2015.06.011

Wang, X., Zhai, P., & Wang, C. (2009). Variations in extratropical cyclone activity in northern East Asia. *Advances in Atmospheric Sciences*, *26*(3), 471–479. https://doi.org/10.1007/s00376-009-0471-8

Wang, Y., Gao, J., Mamtimin, A., Sayit, H., Zhou, C., Li, R., Dawut, M., Yang, F., Huo, W., Wen, C., Song, M., & Aihaiti, A. (2023). Evolution law of atmospheric boundary layer in Gurbantünggüt Desert based on reanalysis dataset and in situ observation data. *Heliyon*, *9*(3), e14147. https://doi.org/10.1016/j.heliyon.2023.e14147

Wen, H. J., Wang, S. L., Wu, C. D., & Liang, M. C. (2024). Association of Asian dust storms and PM2.5 with clinical visits for respiratory diseases in children. *Atmospheric Environment*, *333*, 120631. https://doi.org/10.1016/j.atmosenv.2024.120631

Xu, C., Guan, Q., Lin, J., Luo, H., Yang, L., Tan, Z., Wang, Q., Wang, N., & Tian, J. (2020). Spatiotemporal variations and driving factors of dust storm events in northern China based on high-temporal-resolution analysis of meteorological data (1960–2007). *Environmental Pollution*, *260*, 114084. https://doi.org/10.1016/j.envpol.2020.114084

Yang, X., Shen, S., Yang, F., He, Q., Ali, M., Huo, W., & Liu, X. (2016). Spatial and temporal variations of blowing dust events in the Taklimakan Desert. *Theoretical and Applied Climatology*, *125*(3–4), 669–677. https://doi.org/10.1007/s00704-015-1537-4

Zeng, X., & Dickinson, R. E. (1998). Effect of Surface Sublayer on Surface Skin Temperature and Fluxes. *Journal of Climate*, *11*(4), 537–550. https://doi.org/10.1175/1520-0442(1998)011<0537:EOSSOS>2.0.CO;2

Zeng, Y., Wang, M., Zhao, C., Chen, S., Liu, Z., Huang, X., & Gao, Y. (2020). WRF-Chem v3.9 simulations of the East Asian dust storm in May 2017: Modeling sensitivities to dust emission and dry deposition schemes. *Geoscientific Model Development*, *13*(4), 2125–2147. https://doi.org/10.5194/gmd-13-2125-2020

Zhang, H., Cisse, M., Dauphin, Y. N., & Lopez-Paz, D. (2017). *mixup: Beyond Empirical Risk Minimization* (Version 2). arXiv. https://doi.org/10.48550/ARXIV.1710.09412

Zong, Q., Mao, R., Gong, D.-Y., Wu, C., Pu, B., Feng, X., & Sun, Y. (2021). Changes in Dust Activity in Spring over East Asia under a Global Warming Scenario. *Asia-Pacific Journal of Atmospheric Sciences*, *57*(4), 839–850. https://doi.org/10.1007/s13143-021-00224-7